

MSS RESEARCH LETTERS

Issue #1, May 2018

DISCLAIMER OF WARRANTIES AND LIABILITY

1. While National Environment Agency Meteorological Service Singapore (NEA MSS) has made every reasonable effort to ensure that the information contained in this publication has been obtained from reliable sources, NEA MSS shall not be responsible for any errors or omissions, or for the results obtained from the use of such information.
2. NEA MSS shall also not be liable for any damage or loss of any kind howsoever caused as a result of any reliance on the contents of this publication.

WELCOME ADDRESS

Welcome to the first issue of the Meteorological Service Singapore (MSS) Research Letters. This publication aims at sharing information on research done within MSS, in particular research from the Centre for Climate Research Singapore (CCRS) which forms part of MSS. We hope that the MSS Research Letters (MRL) will act as a conduit for sharing information, knowledge, and experience, as well as foster future collaborations. In doing so, the Research Letters will also act as a repository for MSS research, projects, and in-house development.

The primary pool for MRL contributions is the various branches of CCRS. The Climate Modelling and Prediction branch (CMP) focuses on understanding tropical weather and climate processes, as well as climate change. The Subseasonal and Seasonal Prediction branch (SSP) studies subseasonal and seasonal forecasts for Singapore and the surrounding Southeast Asia region. The Climate and Climate Studies branch (CCS) is in charge of collating and quality control of MSS's weather data. The Weather Modelling and Prediction branch (WMP) works on improving weather forecasts, in particular the SINGV model developed in close collaboration between CCRS and the Meteorological Office in Exeter, UK. The Applied Modelling Branch (AMB) models weather influenced hazards, such as haze and volcanic eruptions. At the Central Forecast Office in Changi Airport, the Weather Services Department (WSD) focuses on applied research for the weather forecasters, and finally the Meteorological Services Department (MSD) works on maintaining our extensive monitoring network.

In this first issue we have contributions covering recent developments in the SINGV model and climatologies of convective areas and wind anomalies around Singapore. Remote as well as regional influences of sea surface temperatures on Singapore rainfall are discussed and an analysis of sources of particles that can lead to haze over Singapore is analysed. These are just a few areas of research at MSS; future issues of the MRL will appear with half year intervals and cover other active areas of investigation. As the newly arrived Director of CCRS I would like to thank everyone who has contributed to this first issue of MRL, in particular thanks to Thea Turkington and Bertrand Timbal who have been instrumental in collecting the contributions and editing the texts.

Erland Källén,
Director of Centre for Climate Research Singapore

EDITOR'S NOTE

After considerable effort by many people, both in MSS and NEA in general, I am proud to present the first issue of the MSS Research Letters. Compared to a standard scientific journal, we wanted to produce a publication centred on the type of research related work done at MSS. The shorter format (termed 'letter') allows for the inclusion of brief studies or preliminary work that may develop into a paper suitable for publication in an international scientific journal. Each letter was reviewed by at least two reviewers, with subsequent discussions between reviewers and authors to allow for a more open review process.

Therefore, a big thank you must go to all the authors for bravely submitting their work and time into this first issue and to all the reviewers for ensuring the quality of the work.

We hope you enjoy and learn from this new endeavour from staff members across MSS and will consider submitting suitable material for subsequent issues.

Warm regards,
Thea Turkington
Editor, MSS Research Letters



TABLE OF CONTENTS

1. Recent developments in SINGV 3
Dipankar, A (WMP, CCRS)

MSS's integrated numerical weather prediction system, SINGV, has been an important in-house development. SINGV has changed much since the initial conception by the UK Met Office and MSS, and both teams are still working hard to improve the system's forecasts. This letter covers the latest three versions of the model and how a few changes can make a big difference in the outcome.
 2. Hourly climatology of convective areas around Singapore from ground-based radar 8
Hassim, M.E. (CMP, CCRS)

Rainfall patterns over Singapore can appear very chaotic, with substantial variation from hour to hour. There are patterns in the chaos, as this letter shows. Here, an hourly climatology of expected frequency of rainfall over Singapore for the various seasons is presented. The work harnesses ground-based weather radar data, which allows for the fine temporal and spatial scale of the rainfall to be studied. The results confirm that yes, indeed there are patterns in the hourly rainfall, and this can be used to help weather forecasters.
 3. Rainfall over Singapore in relation to local and remote sea surface temperatures 15
Heng, B. C. P. (WMP, CCRS), and Gao, E. (CMP, CCRS)

As most Singaporeans know, the 'little red dot' is often affected by what is happening around the world. This is also true for Singapore's rainfall. Patterns in the rainfall on the island can be influenced by large scale patterns in the atmosphere and ocean. This letter examines the relationship between sea surface temperatures (SSTs), both local and remote, to quantify the influence on monthly rainfall. While differences in rainfall can be linked to local SSTs and remote SSTs around the world, the strength, and sometimes even the direction, depend on the time of the year.
 4. Wind anomalies over Singapore and the surrounding region 22
Cheong W. K. (WSD), and Zheng K. (WSD)

This letter focusses on wind patterns during the southwest monsoon and investigates whether deviations in wind can be linked to larger scale processes. Singapore's climate is characterised by two monsoon seasons: the windier and cooler northeast monsoon from December to February, the warmer southwest monsoon from June to October, separated by inter-monsoonal periods. While each of these seasons has their own prevailing wind characteristics, there can be noticeable deviations from year to year. Learning what causes these variations can help us better predict anomalous conditions in the future.
 5. Singapore air history analysis 28
Chong, W.M.E (AMB, CCRS)

Large-scale regional pollution such as transboundary haze episodes can cause discomfort and disruption, but what are the possible geographical source regions impacting Singapore? This letter uses a combination of analysis of historical weather conditions with modelling to 'back trace' the possible source regions of small atmospheric particles. The letter shows that while there are clear patterns based on the time of year, there is also substantial year-to-year variation, meaning that what happened last year is not necessarily a good predictor for this year.
- Glossary 36

RECENT DEVELOPMENTS IN SINGV

Anurag Dipankar

Weather Modelling and Prediction Branch, Centre for Climate Research Singapore

INTRODUCTION

Singapore Variable Resolution (SINGV) is MSS's integrated numerical weather prediction (NWP) system, developed in collaboration with the UK Met Office. The project started in 2013 with the ambitious aim to provide improved forecasts of tropical weather systems in the region. Weather around Singapore is convection-driven, which means it involves interactions between scales as small as turbulent eddies (1 mm) to as large as mesoscale convective systems (100 km). As an NWP model has a resolution typically on the kilometre scale, it has always been challenging to represent convection with reasonable accuracy in such a model (Arakawa and Jung 2011).

Most NWP models have grid resolutions of around 5–10 km and therefore have to use convective parameterisation schemes to represent the interactions between the finer-scale turbulence and large-scale atmosphere. SINGV on the other hand uses a grid resolution of 1.5 km, which is commonly known as a grey-zone (Wyngaard 2004) because in this resolution range convection can neither be fully parameterised nor resolved. This grey-zone resolution poses a challenge to the SINGV development team.

SINGV in its current form does not use any scheme to parameterise convection, rather it depends on the grid to resolve the convection with reasonable accuracy. Despite the issues with resolution, recent updates in the science configuration have shown that SINGV has potential to perform satisfactorily in forecasting weather in the deep tropics. This article focusses on these recent changes in the model and demonstrates how these changes lead to improvements in forecasting rainfall.

MODEL DESCRIPTION AND EXPERIMENT SET UP

SINGV is a tropical version of UK Met Office's NWP system UKV, which is based on a dynamical model called the Unified Model (UM). In total, SINGV has three components. The first component is the dynamical model, UM, which numerically solves a set of prognostic equations for atmospheric variables like temperature,

moisture, and wind, together with parameterisation schemes to represent physical processes like radiation, turbulence, and cloud microphysics, that occur on scales finer than the grid resolution. The details of the numerical model can be found in Davies et al. (2005).

The other two components of SINGV are data assimilation (DA) and an ensemble prediction system (EPS). DA assimilates into SINGV's observational data from different sources, preventing the dynamical model from drifting away from reality. The EPS is designed to account for uncertainties in the initial conditions that the dynamical model starts with. See Lorenc et al. (2000) and Hagelin et al. (2017) for details on DA and EPS, respectively. This study focuses only on changes in the dynamical model (the first component) to isolate the limitations of the dynamical model itself.

As model development requires multiple simulations using different physical and dynamical settings (also called science configurations), long simulations can be very computationally expensive. For this reason, simulations have been performed for August and November 2016 only. These two months were strategically chosen as the weather systems observed in this period were comprised of squall lines, the Southwest Monsoon, and localised convections; all of which are key atmospheric processes affecting rainfall over Singapore. Squall lines that originate from the direction of Sumatra (termed 'Sumatra squalls') are of particular interest because they can bring widespread wet weather and strong gusts to Singapore. While simulating a localised convection is challenging in a kilometre-scale grid model because of their short lifespan and smaller size, Sumatra squalls due to their well-organized structure are expected to be relatively well captured at this scale, and hence serve as a reasonable benchmark to evaluate model performance.

Simulations were performed using a grid resolution of 1.5 km in a domain shown in Fig. 1. Initial and lateral boundary conditions (updated every hour) were interpolated from the Global UM (~25 km) to the SINGV grid (1.5 km). Surface boundary conditions consisted of sea surface temperature (SST) for the ocean points and soil moisture content (SMC) for the land points. SMC data was derived from weekly analysis using data from the UK Met Office's Rainfall Evaporation

Calculation System, while the SST data was derived from OSTIA, the Operational Sea Surface Temperature and Sea Ice Analysis system at the UK Met Office. Starting with the Global UM analysis, forecasts were made for 36 hours using a time step of 60 seconds.

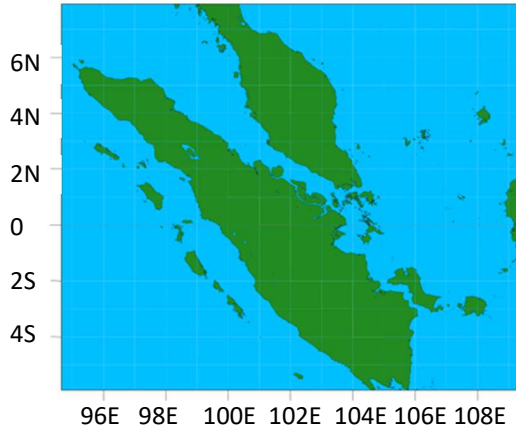


Figure 1. SINGV real-time simulation domain.

Three science configurations were used: (a) SINGV 3.1, which was in real-time until March 2017, (b) SINGV 4.0, in real-time from April 2017 until June 2017, and (c) SINGV 4.1, which replaced SINGV 4.0 in July 2017. The major changes between successive versions and the reasons behind those changes are briefly described below.

Major changes from SINGV 3.1 to 4.0 were the use of a new Prognostic Cloud and Condensate Scheme (PC2, Wilson et al. 2008), as opposed to the previous Smith’s (Smith 1990) diagnostic scheme, and a revised implementation of the stochastic boundary layer (BL) perturbations. These BL perturbations are intended to represent the effects of sub-grid boundary layer turbulence on the triggering of convection. In SINGV 3.1, these perturbations were applied at all grid points using a uniform vertical profile from just above the ground to the top of the BL. While this implementation was

beneficial in terms of objective measures of rainfall skill, on occasions the model would generate chequerboard patterns in near-surface fields, which was potentially problematic in data assimilation trials. In the revised implementation of SINGV 4.0, these perturbations were only applied in the convective boundary layers and the vertical profile was zero at the ground and top of the BL, following a parabolic profile. This implementation eliminated the near surface chequerboard patterns and also follows the implementation used in the UK Met Office version, UKV.

From SINGV 4.0 to 4.1, the major change was the deactivation of the stochastic BL perturbation scheme. This scheme was introduced at SINGV 2.1 and its implementation was changed at each subsequent version (3.0, 3.1, and 4.0). While the scheme initially appeared to improve the simulation of rainfall formation, in subsequent configurations the scheme worsened the simulation of rainfall. The change in the impact of this scheme was presumably due to the influence of the other changes that were added to SINGV, on top of the BL perturbation scheme. The most obvious candidate causing this fundamental change was the use of PC2.

Model performance was evaluated by comparing the predicted rainfall with the rainfall data from the Global Precipitation Measurement (GPM) mission, which comprised various international satellites (Skofronick-Jackson et al. 2017). Due to the difference in resolutions, the output from SINGV was averaged horizontally (“up-scaled”) to the GPM resolution (1°) to make them comparable.

RESULTS AND DISCUSSION

The major improvement in the performance of SINGV came in SINGV 4.0 due to the use of the new cloud scheme (PC2). Figure 2 shows the average

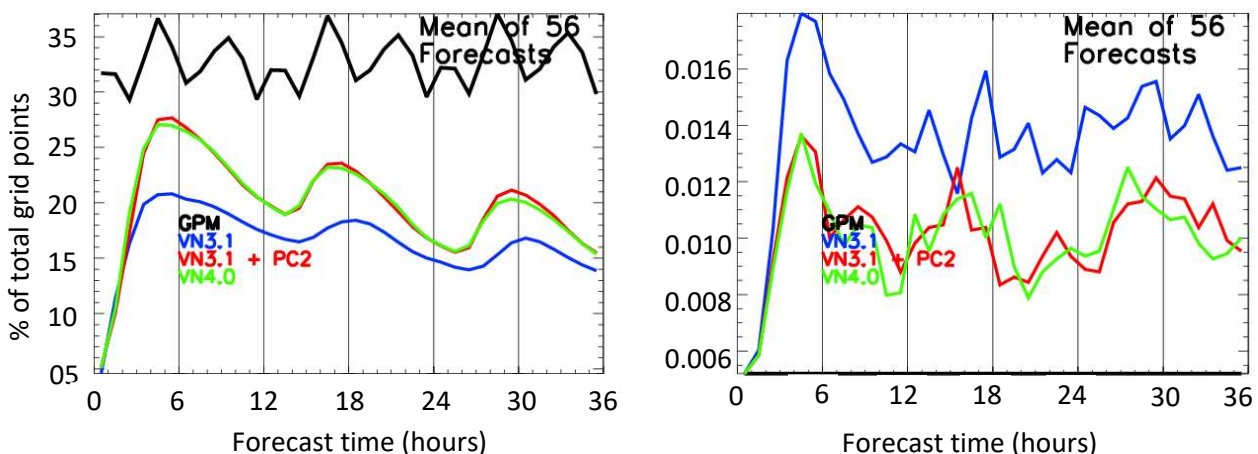


Figure 2. Fraction of grid points versus forecasts time of mean rainfall of 56 forecasts for August 2016 for rainfall rate $R > 0.02$ mm/hr (left) and $R > 50$ mm/hr (right).

percentage of grid points over the entire domain of Fig. 1 that forecast rainfall for light rainfall (>0.02 mm/hr, left) and heavy rainfall (>50 mm/hr, right) for 56 forecasts in August 2016. The 56 forecasts correspond to approximately two forecasts per day. In blue, SINGV 3.1 has too much heavy rainfall and too little light rainfall when compared with the GPM in black. Both SINGV 3.1 with the new PC2 and SINGV 4.0 have significantly reduced occurrences of high intensity rainfall events and increased occurrences of light rainfall (red and green lines, Fig. 2), closer to the GPM results. Note that the black GPM line on the right in Fig. 2 is lying along the abscissa (~0.0056 mm/hr). The low values using the GPM product for heavy rainfall may be due to its resolution being too coarse to capture such heavy rainfall events.

The reduction in intense rainfall is probably a result of decreases in spurious high vertical velocities. Figure 3 shows the number of grid points with vertical velocities exceeding 5 m/s in the entire domain for August 2016 for the different science configurations. It is clear that with the use of PC2 with the SINGV 3.1 configuration, the number of such grid points went down by more than 300%. The reduction in grid points also holds true for SINGV 4.0 in green, which uses the same PC2 scheme.

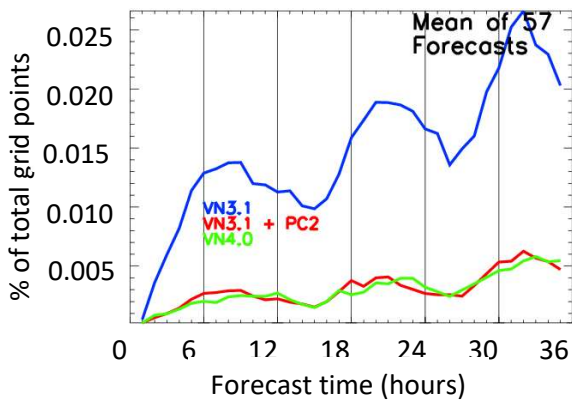


Figure 3. Same as Fig. 2, but for vertical velocity > 5 m/s for August 2016.

The major change in SINGV 4.1 is the deactivation of the stochastic BL perturbation scheme. The impact of this change can be seen in Fig. 4, which compares forecasts from SINGV 3.1 (4b) and 4.1 (4c) with ground-based weather radar (4a) for 6 August, 2016. There is a reduction in the formation of spurious localised convective systems in SINGV 4.1, which was a long-standing issue in SINGV.

The other advantage of removing the BL perturbation scheme is the improvement in the timing of diurnal convection. Figure 5 shows average rainfall

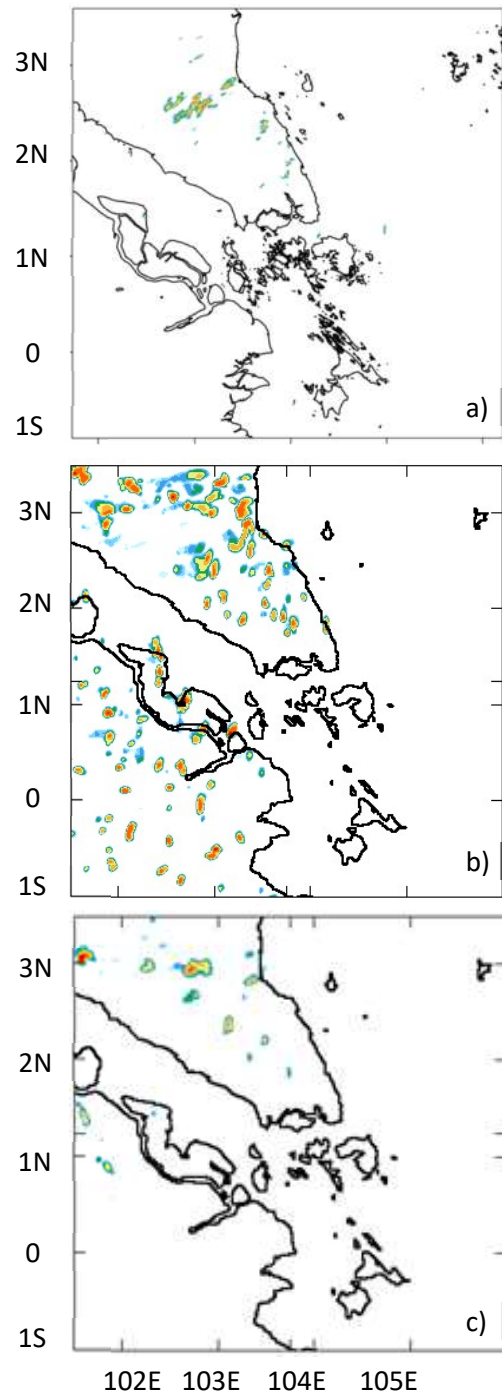


Figure 4. Comparison of accumulated 1-hr rainfall from SINGV 3.1 (b) and SINGV 4.1 (c) with radar (a) on 06 August 2016 at 3 pm local time (07 UTC).

over land of 29 forecasts for August 2016. The GPM rainfall shows a peak 20 hours after the forecast started (4 pm Singapore time). The use of PC2 (blue line) in SINGV 4.0 resulted in an even earlier trigger of daytime convection than in SINGV 3.1 (red line). For SINGV 4.1 (green line), however, the peak rainfall matched the peak of the GPM better. Although there was an improvement in the timing of the peak rainfall in SINGV 4.1, there were still major discrepancies in terms of amount and general timing between modelled and observed rainfall.

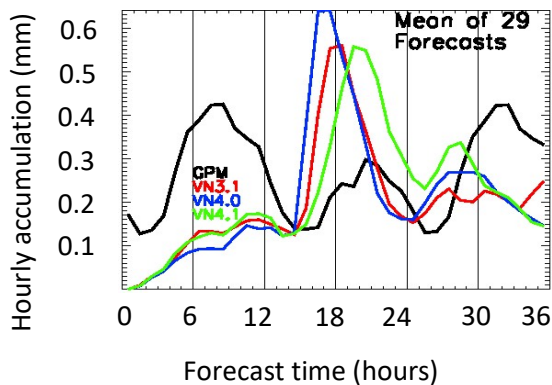


Figure 5. Average rainfall over land for different SINGV versions (see the legend) from 29 forecasts for August 2016. All were initialised at 12 UTC.

Finally, in order to demonstrate the improvement in SINGV 4.1 in capturing Sumatra squalls, Fig. 6 shows the rainfall maps on 19 August 2016 when a squall line passed over Singapore at approximately 9 am local time. Here, Fig. 6a is the image from radar and the other two panels are SINGV 3.1 (6b) and 4.1 (6c). The two model forecasts are for T+25 after the initialisation time at 00 UTC 18 August 2016. From Fig. 6 it is evident that while SINGV 3.1 failed to capture the event, SINGV 4.1 did better in terms of timing and spatial coverage of the rainfall over Singapore. Although

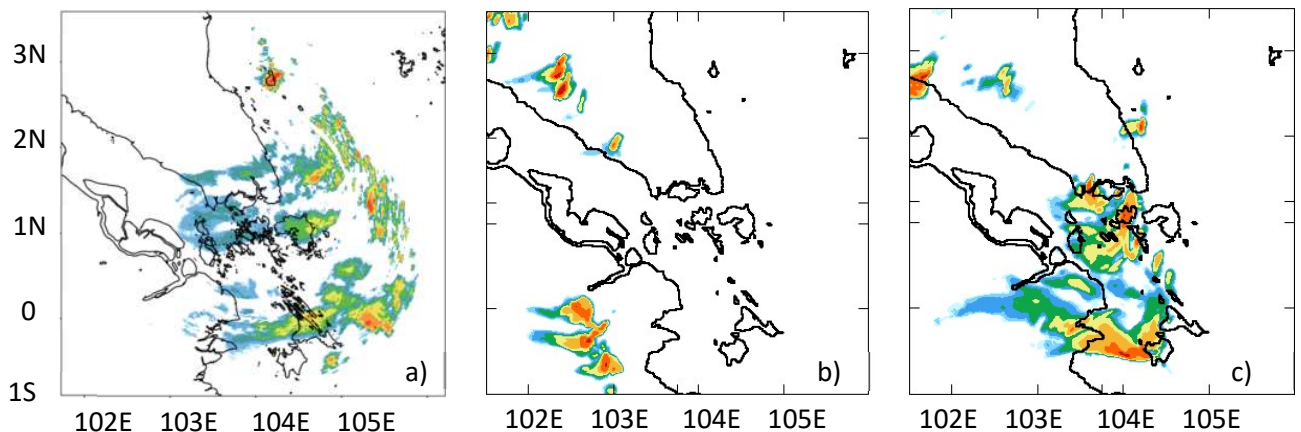


Figure 6. Rainfall maps on 19 August 2016 at 9 am local time (01 UTC) for radar (a), SINGV 3.1 (b) and SINGV 4.1 (c).

only one case is shown here, more of such cases can be found in SINGV 4.1 report by Webster et al. (2017).

SUMMARY

Relative performances of the three recent configurations of SINGV (4.1, 4.0, and 3.1) were assessed against the rainfall data from GPM and Singapore’s weather radar. Results show that SINGV 4.1 is significantly better than SINGV 3.1 in many respects. SINGV 4.1 reduced occurrences of spurious convective rainfall that existed in all previous SINGV versions, improved the diurnal timing by reducing the delay of the diurnal peak of convection by 3 hours, and improved the structure and timing of squall lines. With respect to SINGV 4.0, improvements in SINGV 4.1 were mainly in reducing the delay in the peak of diurnal convection. While improvement in the timing of the diurnal peak was due to the removal of the BL perturbation scheme, the other two improvements were due to the use of the new PC2 cloud scheme.

As already discussed, simulating a squall line is relatively easier than a localised thunderstorm at kilometre-scale. The current SINGV version shows potential for better forecasts of the squall lines, but more work is needed to make SINGV useful for simulating localised thunderstorms, which are known to produce very high-intensity rainfall in a short span of time leading to flash floods. Fundamental work is still needed, locally as well as internationally, to understand the modelling biases in the deep tropics so that relevant measures can be taken to improve the model performance.

ACKNOWLEDGEMENTS

The author would like to thank the entire SINGV team in Singapore and at the UK Met Office for their hard work in getting SINGV to its present stage.

REFERENCES

Arakawa, A. and Jung, J.H. (2011) Multiscale modelling of the moist-convective atmosphere—A review. *Atmospheric Research*, 102:263–285.

Davies, T. Cullen, M.J.P., Malcolm, A.J., Mawson, M.H., Staniforth, A., White, A.A., and Wood, N. (2005) A new dynamical core for the Met Office's global and regional modelling of the atmosphere. *Quarterly Journal of the Royal Meteorological Society*, 131:1759–1782.

Hagelin, S. Son, J., Swinbank, R., McCabe, A., Roberts, N., and Tennant, W. (2017) The Met Office convective-scale ensemble, MOGREPS-UK. *Quarterly Journal of the Royal Meteorological Society*, 143:2846–2861.

Lorenc, A.C., Ballard, S.P., Bell, R.S., Ingleby, N.B., Andrews, P.L., Barker, D.M., Bray, J.R., Clayton, A.M., Dalby, T., Li, D. et al. (2000) The Met. Office global three-dimensional variational data assimilation scheme. *Quarterly Journal of the Royal Meteorological Society*, 126:2991–3012.

Skofronick-Jackson, G., Petersen, W.A., Berg, W., Kidd, C., Stocker, E.F., Kirschbaum, D.B., Kakar, R., Braun, S.A., Huffman, G.J., Iguchi, T. et al. (2017) The Global Precipitation Measurement (GPM) Mission for Science and Society. *Bulletin of the American Meteorological Society*, 98:1679–1695.

Smith, R.N.B. (1990) A scheme for predicting layer cloud and their water content in a general circulation model. *Quarterly Journal of the Royal Meteorological Society*, 116:435–460.

Webster, S., Dipankar, A., and Sanchez, C. (2017) SINGV 4.1 report. *SINGV technical report*.

Wilson, D.R., Bushell, A.C., Kerr-Munslow, A.M., Price, J.D., and Morcrette, C.J. (2008) PC2: A prognostic cloud fraction and condensation scheme. I: Scheme description. *Quarterly Journal of the Royal Meteorological Society*, 134:2093–2107.

Wyngaard, J.C. (2004) Toward Numerical Modelling in the “Terra Incognita”. *Journal of Atmospheric Science*, 61:1816–1826.

HOURLY CLIMATOLOGY OF CONVECTIVE AREAS AROUND SINGAPORE FROM GROUND-BASED RADAR OBSERVATIONS

Muhammad Eqmal Hassim

Climate Modelling and Prediction Branch, Centre for Climate Research

INTRODUCTION

As part of daily operations in the Weather Services Department (WSD) of Meteorological Service Singapore (MSS), the duty meteorologist for aviation weather is required to issue forecasts for airports and surrounding areas. A core task is the provision of timely warnings and updates for any ongoing or expected occurrence of severe convection (i.e. thunderstorm activity) nearby. This task is normally achieved through close monitoring of weather phenomena using data from satellites (such as from Himawari-8, a Japanese geostationary weather satellite) and also ground-based weather radar, complemented with numerical weather prediction (NWP) models. Driven by the increase in air traffic volume, the need for more precise forecasts of thunderstorm probability in the vicinity of Singapore for the next 1- to 6-hour window has become more critical. Severe weather can be disruptive to air traffic operations, as potential threats from thunderstorms include lightning, microbursts, and the associated low-level wind shear from a storm's outflow.

To meet users' requirements, a climatological study of convective areas around Singapore using ground-based radar reflectivity data is needed. A key outcome is the provision of hourly maps documenting the probability of convective areas occurring within 100 km of the Changi weather radar based on the mean or expected frequency from past events. The information contained within these hourly maps serve as a preliminary reference point for the issuance of short-term convective weather forecasts, as they can be combined with current analysis and very high-resolution NWP output of near-term conditions.

This letter describes the data and methods used, discusses the hourly radar-based climatology obtained, and presents a summary along with future work planned.

DATA AND METHOD

CHANGI S-BAND POLARIMETRIC RADAR DATA

This study utilised the 2011–2014 radar reflectivity data obtained from the S-band, dual-polarised Doppler weather radar system situated near Changi International Airport at 1.4°N, 103.8°E. Due to technical constraints in processing the raw data, only four years of data were readily available when commencing the analysis. The current Changi radar was commissioned in April 2010 and produces three-dimensional volume scans of the surrounding atmosphere, detecting precipitation-sized particles within a radius of 240 km every five minutes. The main operational scanning strategy uses a series of eight elevation sweeps, or tilt angles, from 1° to 40° as shown in Fig. 1. A long range weather surveillance scan is also conducted at 0.3° out to a range of 480 km after the main scan is done. The S-Band radar has an approximately 10 cm wavelength, a 1° beam width and a range resolution of 250 m.

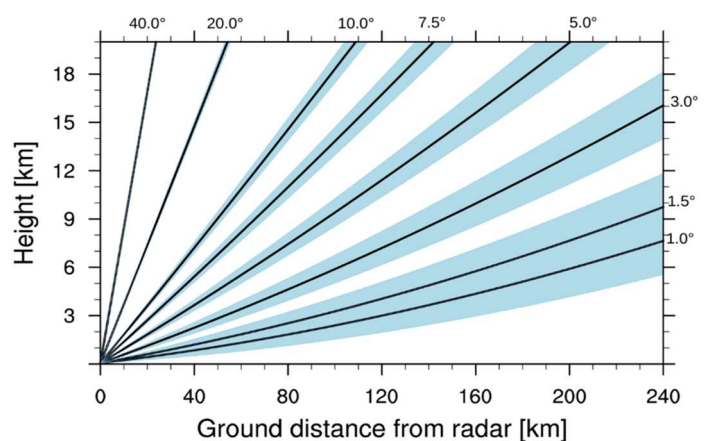


Figure 1. The operational scanning strategy of the Changi Weather Radar (8 elevation angles from 1° to 40°). The solid black lines are the beam centres while the blue shade represents the coverage of the 1° beam width with distance from Changi radar (left), which is 59 m above sea level.

Prior to the analysis, the RainDART application from SELEX ES-GmbH (vendor of the Gematronik Weather Radar Systems used by MSS) was used to interpolate volumetric reflectivity data (in spherical coordinates of azimuth, elevation and range) to a constant height level of 2.5 km with a 1 km × 1 km horizontal grid spacing. This constant altitude plan position indicator (CAPPI) gridded product forms the basis for identifying convective and stratiform pixels in the reflectivity field. A sample CAPPI field is shown in Fig. 2a. The effective horizontal range of the 2.5 km CAPPI gridded product is ~100 km, as it is constrained by the corresponding ground distance where the beam height of the lowest tilt angle (1° in the main volume scan) reaches the 2.5 km altitude (Fig. 1).

The 2.5 km height level was chosen because the altitude is sufficiently high enough to eliminate possible ground clutter effects and low enough to avoid contamination from the “bright band” (high reflectivity) layer in heavy stratiform precipitation. In the equatorial tropics, the “bright band” signature typically occurs between the 4–5 km altitude, just below the melting (0°C) level. This bright band is the region in which ice particles begin to melt and get coated with a layer of liquid water. The much higher reflective power of water (about 10 times more compared to ice) gives this layer of wet melting ice its high radar echo returns (thus giving the “bright band” effect).

CONVECTIVE/STRATIFORM CLASSIFICATION

The Steiner algorithm (Steiner et al. 1995) was used to objectively classify the gridded 5-min reflectivity data (in dBZ) into convective and stratiform pixels. The algorithm was developed using radar data over Darwin in tropical northern Australia, covering both the active monsoon and the break periods. Rainfall over Darwin is highly convective in nature during the monsoon breaks. The technique is a texture-based method that analyses the horizontal gradient of the radar reflectivity field and searches for peaks in the measured reflectivity. The method is therefore platform independent. The 2-step algorithm works in the following way:

- i. First, any pixel within the horizontal radar grid is identified as automatically convective if it has a reflectivity value of ≥ 40 dBZ, or its value exceeds a threshold, ΔZ (known as the peakedness criterion), which varies depending on Z_{bg} , the area-averaged background reflectivity. Z_{bg} is calculated within a 12 km radius around a pixel. In the analysis, the modified peakedness criterion suggested by Penide et al. (2013) was adopted, given by

$$\Delta Z = 12 - (Z_{bg}^{2.05} \div 180) \quad (1)$$

where $0 \leq Z_{bg} \leq 42.43$ dBZ.

The modified criterion (Eq. 1) reduces the misclassification of isolated convective grid points embedded within stratiform areas by about 50% when compared to the original Steiner formulation (Penide et al. 2013).

- ii. Once a convective centre has been identified, neighbouring grid points are then classified as convective areas if they lie within a diagnosed radius of influence. This convective radius is a function of the average background reflectivity, Z_{bg} , which increases by 1 km for every 5 dBZ between 20–40 dBZ. Finally, the remaining non-zero reflectivity values are subsequently classified as stratiform.

Note that 40 dBZ is the accepted minimum threshold for classifying a radar echo pixel as convective, as rain rates from this high intensity value cannot be stratiform, which are typically less than 10 mm/hr (Leary and Houze 1979; Kumar et al. 2011; Penide et al. 2013). Analysing drop size diameter measurements from 9 rain events over Singapore (SG), Kumar et al. (2011) also found that convective rainfall typically has rain rates > 10 mm/hr and reflectivities > 37 dBZ.

MEAN HOURLY CONVECTIVE PROBABILITY AT EACH GRID POINT

After classifying the reflectivity field into convective and stratiform areas (Fig. 2b), hourly totals at each grid point were computed by summing the number of convective pixels that occurred in the 5-min data for every clock hour. For example, the occurrences between 08–09 UTC (16–17 LT) were summed under 08 UTC (16 LT). The hourly summation was done for every day in the dataset. Finally, the 1 hr climatology (based on mean frequency) was obtained by averaging the aggregate amount over the corresponding number of days available in the 4-year sample for the stipulated clock hour. This 1 hr climatology yields the probability that a location had a convective cell sometime during that hour (Eq. 2).

$$\begin{aligned} Pr_{cv}(x, y, M, h) \\ = \frac{1}{N_h} \sum_1^{N_h} I_{cv}(x, y, M, h) \end{aligned} \quad (2)$$

where M is month, h is the UTC hour, I_{cv} is the sum of convective pixels at point x, y for UTC hour h and N is the number of M days for the corresponding UTC that is available in the 4-year dataset. The calculation was repeated separately for each calendar month. An example is shown in Fig. 2c for 08 UTC (16 LT) for the month of January.

For the 4-year sample used, the maximum number of available days for each UTC hour varies from 112 to 124 days, depending on the calendar month. There were some missing hours in the dataset, which meant that some individual hours were divided by less than the maximum number of days possible.

RESULTS AND DISCUSSION

APPLICATION OF THE CONVECTIVE-STRATIFORM SEPARATION METHOD: AN EXAMPLE

To illustrate how the classification algorithm works, Fig. 2a shows a sample reflectivity field at the 2.5 km height level taken from 29 January 2011 at 0828 UTC (1628 LT). At this time, there is significant

weather activity detected within the radar domain that is likely associated with a monsoonal cold surge event. The radar observations show extensive areas covered by moderate to high reflectivity echoes with values ranging from 15–35 dBZ (green shades). These large regions are identified as being stratiform by the algorithm (Fig. 2b, grey shade).

Pockets of much higher reflectivity values exceeding 40 and 50 dBZ are also seen in Fig. 2a (light orange to red shades). These pockets occupy relatively smaller areas and are mainly embedded within the larger stratiform region (Fig. 2b). The algorithm identifies these pockets of more severe intensities as convective pixels. Clearly, these are areas with the heaviest rainfall and indicate the presence of intense convective cells where there exists strong updrafts and downdrafts. Note the technique has also classified reflectivity pixels slightly less than 40 dBZ as convective. These lower reflectivity convective pixels can be attributed to the peakedness criterion described above. In this particular snapshot, 4.9% of the radar domain is covered by convective areas, while stratiform regions cover 48.2%.

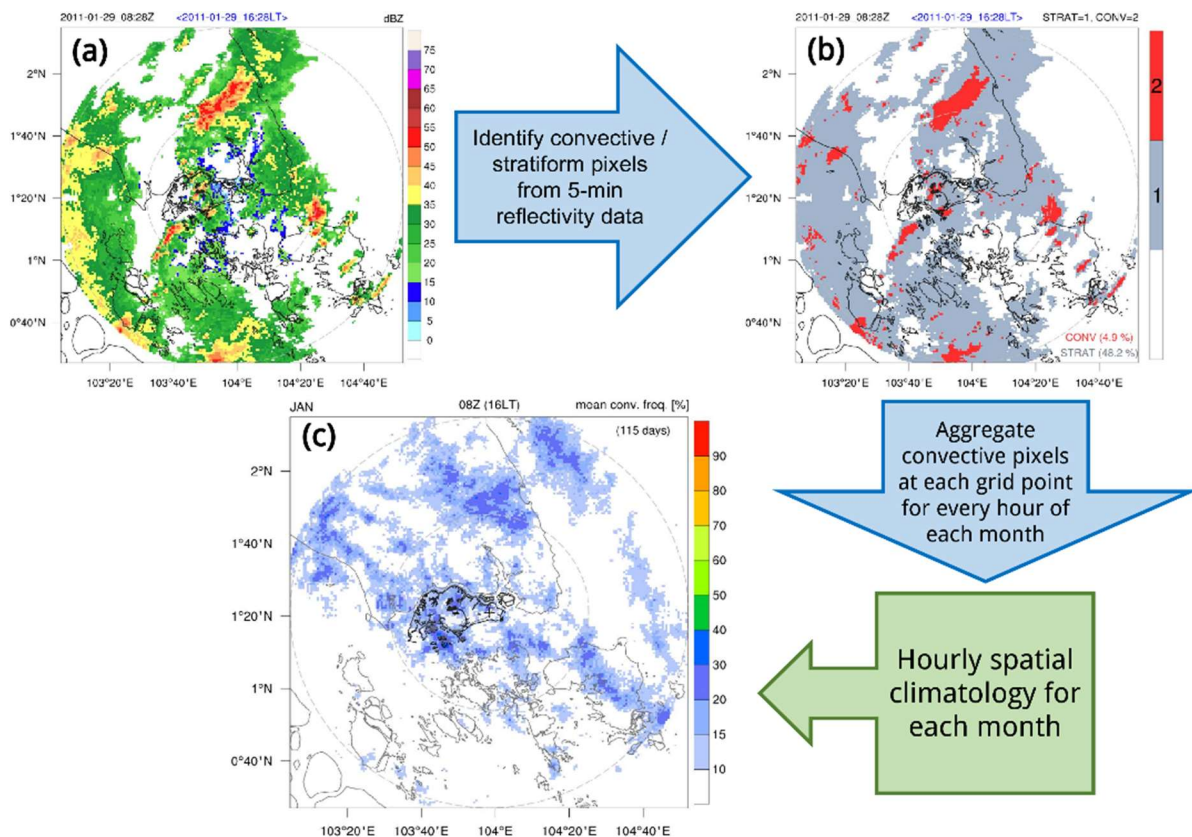


Figure 2. Schematic of the analysis procedure undertaken. Shown is an example of (a) a 5-min reflectivity CAPPI field (dBZ) and (b) the corresponding Steiner classification of convective (red) and stratiform (grey) areas. (c) shows the resulting climatology for hour 08 UTC / 16 LT in January over the 2011–2014 period.

HOURLY CLIMATOLOGY FOR EACH CALENDAR MONTH

Computing the mean hourly convective frequency for each grid point allows us to build a diurnal climatology of thunderstorm probability for the region. However, as Singapore experiences different large-scale meteorological flow patterns depending on the time of year, a separate hourly climatology was constructed for each calendar month. The climatologies give us a statistical understanding of how convective areas around Singapore are distributed throughout the day in various months. The mean convective frequency (in %) can be interpreted as the probability of convective occurrence over a location for the chosen hour, i.e. the chance a convective cell occurs over an area within that hour on any given day of the stipulated month. Thus, the climatological spatial maps highlight when certain areas are much more prone to convective storms.

The climatologies in Fig. 3 all display to some extent a diurnal cycle of convective frequency over land driven by strong surface heating during the day (middle rows) and radiative cooling at night (upper and lower rows). On the other hand, observed spatial variations between the months are arguably the result of interactions between the prevailing background wind, which vary in direction and magnitude with season, and sea breezes from strong daytime heating of land. This suggests an intrinsic statistical pattern of convective events over the domain and possibly over a wider region at different times of the year. Such probabilistic areal information would be useful as forecast guidance.

As an example, selected hourly climatology spanning a 24-hour period are shown for December, April and August (Fig. 3). These months are representative of the time of year when Singapore experiences the Northeast (NE) Monsoon, inter-monsoon (IM), and Southwest (SW) Monsoon, respectively. Mean low-level winds during the NE Monsoon are generally from the north-northeast or northwest, while they prevail from the southwest or southeast during the SW Monsoon. Weak and variable winds characterise the IM months, especially in April.

Focusing on the selected months, at 21 UTC (05 LT) in December, convective locations are largely confined to the eastern coastal areas of Johor north of Singapore and near the Riau islands to the south and southwest of Singapore. Contrast this with convective locations for the same hour in April and August, which are largely concentrated over the Straits of Malacca to the west of Singapore. Most of this region has a 15–40% probability of convective occurrence, with more cells likely to happen in April than in August. The more

frequent early morning offshore convection in April is likely the result of convergent land breezes originating from Sumatra and Peninsular Malaysia, which tend to develop in quiescent background wind conditions and strong night time cooling over land due to relatively clear skies.

At 05 UTC (13 LT), convective areas in April and August become more prominent over land, especially over the eastern coast of southern Malay Peninsula (Johor) and over Bintan island. Specifically, there is a very high (80–90%) chance of thunderstorms occurring over Bintan between 05–06 UTC / 13–14 LT every day in April (and May, not shown). In other words, deep convection can be expected to occur in the early afternoon over the Bintan region almost every day in those months. Such frequent occurrence is likely due to the convergence of sea-breezes over relatively flat terrain, which are favourably generated by strong land surface heating in light and variable wind conditions. The situation over Bintan in April is highly reminiscent and likely analogous to that over the Tiwi Islands, near Darwin, where deep afternoon thunderstorms (locally known as ‘Hector’) are generated almost every day by the organisation of shallow convection and strong convergence resulting from the collision/confluence of island-scale sea breeze fronts in moist unstable conditions during the build-up and break monsoon phases (e.g. Keenan et al. 1990; Carbone et al. 2000; Crook 2001).

By late afternoon (09 UTC, 17 LT), there is reduced probability of strong convection in the eastern quadrants of the radar domain during December and April. At the same time, convective probability has increased substantially over the inland areas of Johor and Singapore, especially over northern, central, and western parts. The area directly north of Singapore is a particular hotspot in April. In contrast, convection is more likely to occur over the eastern coast of Johor in August. Note that the August convective spatial pattern is opposite to that seen in December, which is concentrated over the western coastal areas. Sea breezes over those respective locations in December and August tend to oppose the prevailing wind direction at this time, promoting low-level convergence and convective initiation and subsequent development. Finally, there is very little thunderstorm probability within the radar domain at night (21 LT, 13 UTC) in all months shown here.

A bi-monthly climatology has also been computed for each hour (Fig. 4) by combining consecutive months in adjacent pairs (Dec–Jan, Apr–May, Aug–Sep; other 3 pairs not shown). Groupings

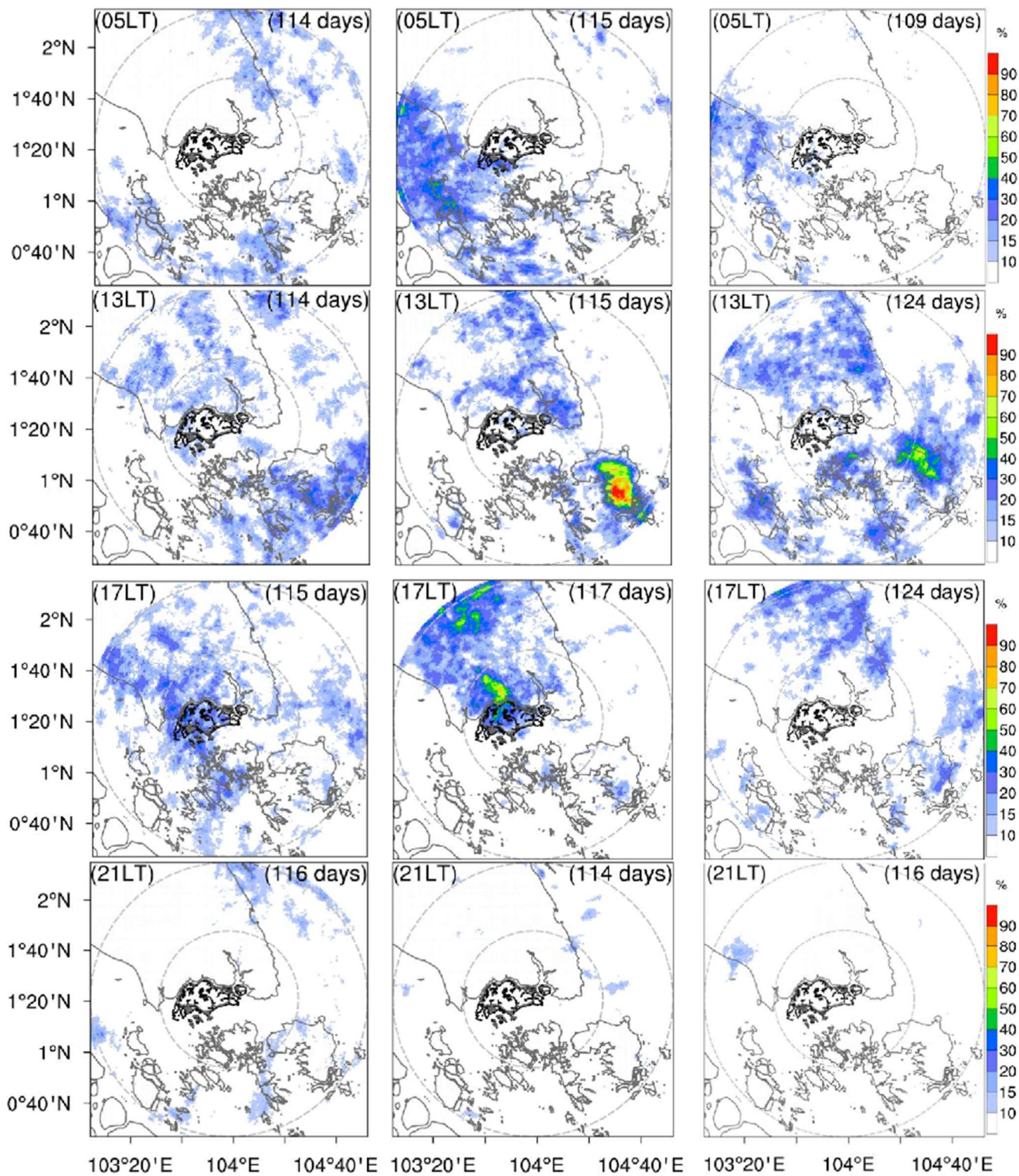


Figure 3. Diurnal evolution of convective areas for December (left column), April (centre) and August (right) as shown by selected hourly climatology of mean convective frequency (%): top row - 21 UTC (05 LT), 2nd row - 05 UTC (13 LT), 3rd row - 09 UTC (17 LT) and bottom 18 UTC (21 LT), respectively. The number of days that make up the sample for the chosen hour is shown in brackets at the top right hand corner of each panel.

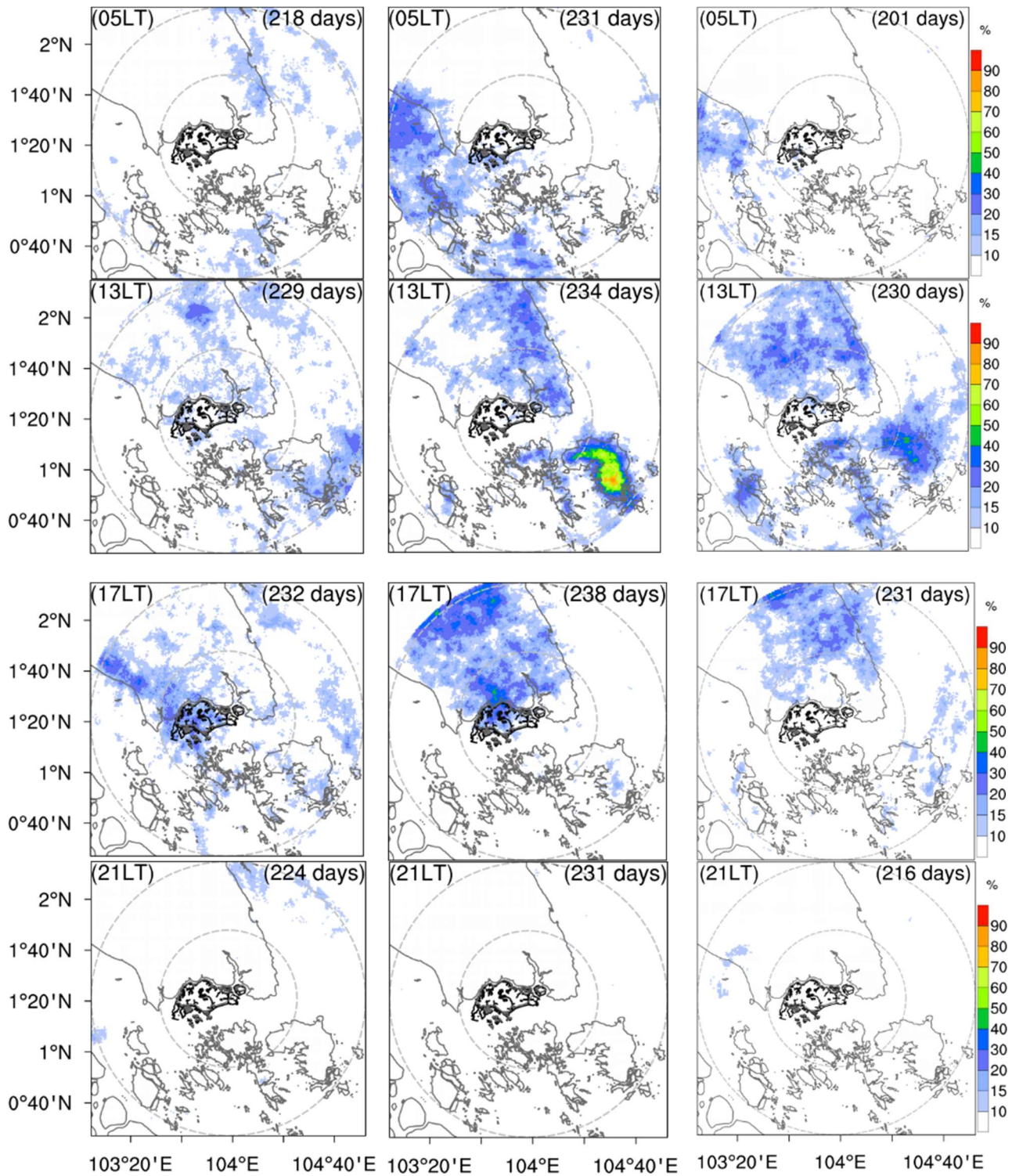


Figure 4. As in Fig. 3 but for combined months of December-January (left), April-May (centre) and August-September (right).

are based on visual inspection of the spatial distribution of hourly convective areas and months that have broadly similar spatial characteristics are paired together. This grouping approximately doubles the sample size for each hour considered, giving a more robust estimate of the occurrence probability. In doing so, it was assumed that the similarity in spatial patterns between the paired months arise from similar flow and thermodynamic conditions given that the months are from the same season.

While a 4-year dataset may be considered too short for a robust climatology, it is worth noting that except for 2011 (La Niña year), the radar dataset used in this climatological study consist of years when the El Niño-Southern Oscillation (ENSO) cycle is in a neutral phase. Hence, the hourly climatology produced is assumed to be largely representative of normal meteorological conditions not complicated by El Niño or La Niña effects.

CONCLUSION

To help improve aviation weather forecasts, monthly and bi-monthly series of hourly spatial maps were constructed to depict the climatological probabilities of convective area occurrence based on weather radar from 2011–2014. These maps show regions of thunderstorm potential every hour within a radius of ~100 km around Singapore. They are intended to serve as a preliminary reference point and guidance tool for operational meteorologists, particularly those working in aviation weather services. The climatological maps suggest that there is a degree of organisation of convective events around Singapore based on ground-radar observations. These maps can be combined on a daily basis with NWP guidance and current analysis for better short-term (1 to 6-hour window) forecasts of areas with thunderstorm potential.

Efforts to extend the dataset to include more recent years (2015–2017) for a more robust climatology are ongoing. Future work planned includes mapping the distribution of the intensity of convective areas to get a sense of where the most severe storms tend to occur over the domain, and if there are any seasonal variations. This work is in addition to exploring the spatiotemporal distribution of both convective and stratiform rain observed by radar, to better understand the rainfall climate over Singapore.

ACKNOWLEDGMENTS

The author would like to acknowledge Yap Kar Lin from the Weather Services Department of Meteorological Service Singapore, for fruitful discussions on the requirements and challenges for aviation forecasting and for her comments on an early version of the manuscript.

REFERENCES

- Carbone, R., Wilson, J.W., Keenan, T.D., and Hacker, J.M. (2000) Tropical Island Convection in the Absence of Significant Topography. Part I: Life Cycle of Diurnally Forced Convection. *Monthly Weather Review*, 128:3459–3480.
- Crook, N.A. (2001) Understanding Hector: The Dynamics of Island Thunderstorms. *Monthly Weather Review*, 129:1550–1563.
- Keenan, T.D., Morton, B.R., Zhang, X.S., and Nguyen, K. (1990) Some characteristics of thunderstorms over Bathurst and Melville Islands near Darwin, Australia. *Quarterly Journal of the Royal Meteorological Society*, 116:1153–1172.
- Kumar, L.S., Lee, Y.H., Yeo J.X., and Ong, J.T. (2011) Tropical Rain Classification and Estimation of Rain from Z-R (Reflectivity-Rain Rate) Relationships. *Progress in Electromagnetics Research B*, 32:107–127.
- Leary, C.A. and Houze, R.A. (1979) Melting and Evaporation of Hydrometeors in Precipitation from the Anvil Clouds of Deep Tropical Convection. *Journal of the Atmospheric Sciences*, 36:669–679.
- Penide, G., Protat, A., Kumar, V.V., and May, P.T. (2013) Comparison of Two Convective/Stratiform Precipitation Classification Techniques: Radar Reflectivity Texture versus Drop Size Distribution-Based Approach. *Journal of Atmospheric and Oceanic Technology*, 30:2788–2797.
- Steiner, M., Houze, R.A., and Yuter, S.E. (1995) Climatological Characterization of Three-Dimensional Storm Structure from Operational Radar and Rain Gauge Data. *Journal of Applied Meteorology*, 34:1978–2007.

RAINFALL OVER SINGAPORE IN RELATION TO LOCAL AND REMOTE SEA SURFACE TEMPERATURES

Boon Chong Peter Heng¹ and Elaine Gao²

¹Weather Modelling and Prediction ²Climate Modelling and Prediction Branch, Centre for Climate Research Singapore

INTRODUCTION

The El Niño–Southern Oscillation (ENSO) is an atmospheric-oceanic phenomenon connected with the weakening (during El Niño) or strengthening (during La Niña) of the Walker circulation over the equatorial Pacific. The impacts of ENSO on precipitation across the globe are well documented (e.g. Ropelewski and Halpert 1987). While rainfall over the Maritime Continent is significantly influenced by ENSO, there are seasonal variations in the strength and coherence of the relationship (Hendon 2003; McBride et al. 2003; Chang et al. 2004; Tangang and Juneng 2004). In Singapore, based on preliminary studies using rainfall data from five meteorological stations spanning 50 to 60 years, Cheong (2013) found that rainfall in the dry Southwest Monsoon period (JJAS) tends to be lower (higher) than the long-term mean during El Niño (La Niña) episodes, but the reverse is true in the wet phase of the Northeast Monsoon (DJF).

The relationship between reduced rainfall and El Niño conditions during the dry season (JJA) is spatially-coherent and consistent across the Maritime Continent. Hendon (2003) proposed a feedback mechanism, in which anomalously warm SSTs in the central Pacific enhance surface easterlies over the Maritime Continent,

increasing evaporative cooling and enhancing local SST cold anomalies and further reducing dry season rainfall. The reverse relationship observed for Singapore during the wet season is, however, inconsistent across the Maritime Continent. Whereas Tangang and Juneng (2004) did indeed find a strong negative correlation between wet season rainfall in Malaysia and local/remote SST anomalies, Hendon (2003) showed that wet season rainfall in Indonesia is uncorrelated with local/remote SST. Separate mechanisms have been proposed to explain these contrasting correlations during the wet season, but it is uncertain from preliminary studies alone to what extent these may be appropriate for Singapore. Hence, to better understand the seasonally varying ENSO impact on rainfall over Singapore, and to separate out the influence (if any) of local and remote factors, we examine the relationships between local rainfall and sea surface temperatures (SSTs) in the western Maritime Continent as well as in the central equatorial Pacific.

DATA AND METHODS

This study uses the monthly rainfall data averaged over three rain gauge stations, S6, S7, and S23, from September 1956 through August 2016 (hereafter

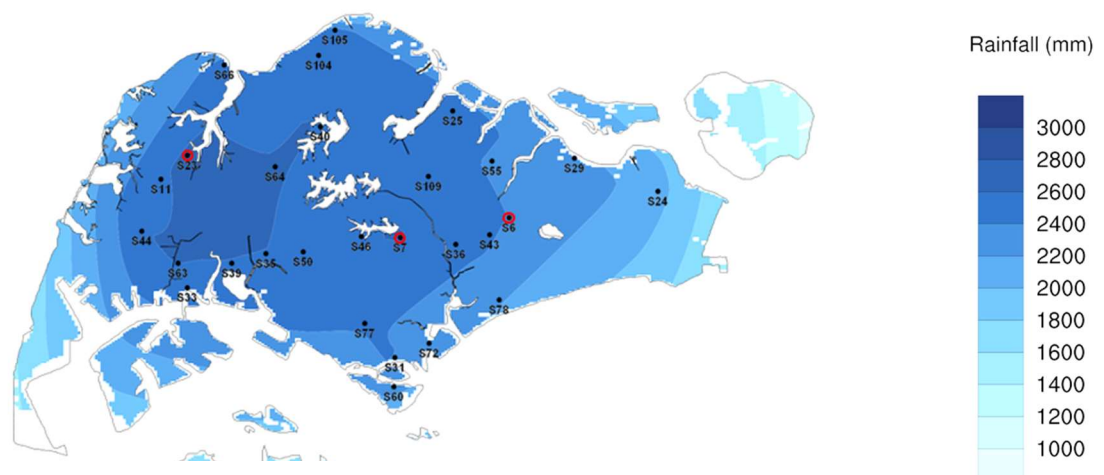


Figure 1. Map of Singapore showing the climatological annual rainfall distribution (1981–2010) and the locations of the 28 rainfall stations used for climate monitoring. The three stations with monthly rainfall records going back to at least 1955 are circled in red.

SgP03) as the rainfall index for Singapore. Analyses of ENSO-driven rainfall anomalies require long records of rainfall and SSTs as ENSO events have a return period of between two and seven years. Of the 28 rainfall stations in Singapore used for climate monitoring (shown in Fig. 1), only the SgP03 stations have monthly rainfall records going back to at least 1955. By virtue of their locations (red circles, Fig. 1), the monthly rainfall averaged over these stations are a good proxy for rainfall over Singapore (Fig. 2).

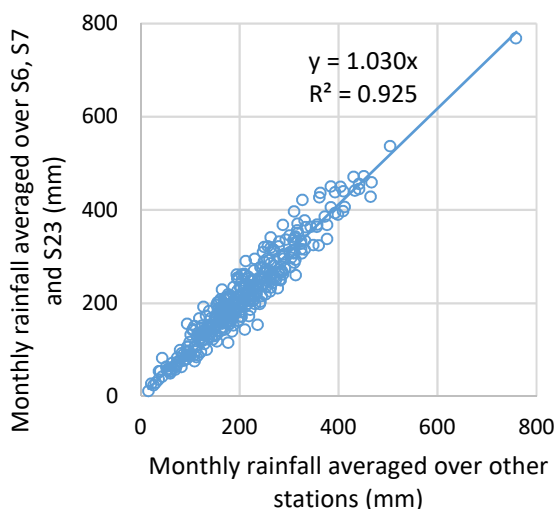


Figure 2 Scatterplot of monthly rainfall averaged over rain gauges S6, S7, and S23, against average rainfall at the other 25 stations for 1981–2010. The best-fit linear regression line (forced through the origin), the regression slope, and the explained variance are also included.

SST data are from the NOAA Extended Reconstructed SST, version 5 product (ERSSTv5; Huang et al. 2017) and are comprised of in situ observations

from ships, buoys and Argo floats. Compared to ERSSTv4, the new product has a better representation of spatial variability over the global oceans and the magnitude of ENSO events, both of which are important considerations for this study. The complete ERSSTv5 dataset is from 1854 to present. By selecting the period 1956 to 2016, the large uncertainties associated with the SST analyses prior to 1950 due to the relatively sparse observations are avoided. Using this SST dataset, within the 60-year study period, we have had 22 (18) El Niño (La Niña) DJF seasons, based on the Oceanic Niño Index (ONI) published by NOAA (NOAA 2018).

To identify the tropical Indo-Pacific regions within which interannual variability in Singapore rainfall is most strongly associated, the correlation was calculated between seasonal SgP03 and seasonal mean SST at each grid point in the region 40° N, 40° S, 40° E, 70° W. The Pearson’s correlation coefficient and subsequent analyses were calculated using the KNMI Climate Explorer tool (KNMI 2018).

To investigate more closely the relationship between local SSTs and rainfall over Singapore, and to enable comparison with Tangang and Juneng (2004), the Pearson’s correlation coefficient was calculated for monthly SgP03 with two local SST indices representing respectively the South China Sea (0°, 10°N, 100°E, 116°E; ScsSST) and the Indonesian seas (10°S, 0°, 90°E, 120°E; IndoSST). Similar correlations with SST over the remote Niño 3.4 region (5° S, 5°N, 170°W ,120°W; Nino3.4) were calculated to study the influence of central equatorial Pacific SSTs on Singapore rainfall. The oceanic regions underlying the SST indices are demarcated in Fig. 3 over

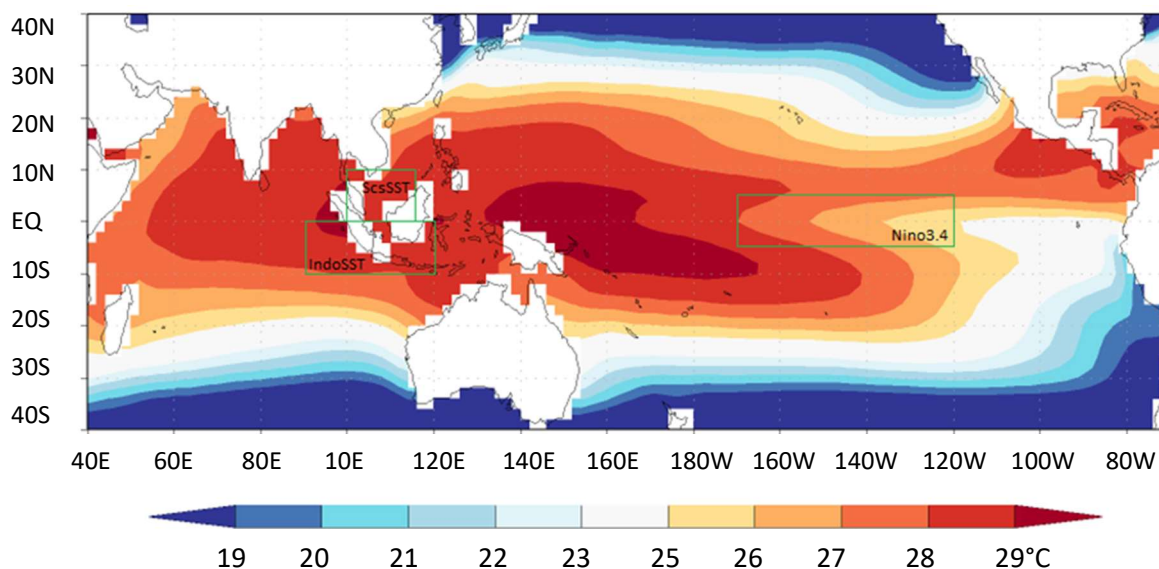


Figure 3. The annual (Jan-Dec) mean SST (1957–2016) over the tropical Indo-Pacific (°C). The oceanic regions underlying the ScsSST, IndoSST, and Nino3.4 SST indices are outlined in green.

the background annual mean SST between 1957 and 2016.

Since ENSO is a key driver of interannual variability in regional SSTs, the correlations between SgP03 and local SSTs could be due to ENSO's influence on both. For this reason, partial correlations were calculated between SgP03 and the SST indices based on the correlations between local and Nino3.4 SST anomalies. The partial correlation of A with B, where their linear relationships with C is removed ($r_{AB.C}$), is given by:

$$r_{AB.C} = \frac{r_{AB} - r_{AC}r_{BC}}{\sqrt{(1-r_{AC}^2)(1-r_{BC}^2)}} \quad (1)$$

The partial correlations are indicative of the rainfall variability that is explained by local SST anomalies independent of SST variability in the central equatorial Pacific and vice versa.

All of the correlation analyses were performed with data detrended by removing the long-term linear trend from each index and SST grid point. The long-term trends were calculated based on data spanning 1956–2016.

RESULTS AND DISCUSSION

SEASONAL CORRELATION MAPS

The maps of correlation between SgP03 and SST fields in Fig. 4 highlight, for each season, the oceanic regions with which interannual variability in Singapore rainfall is associated.

During MAM, SgP03 is weakly correlated with northwestern Pacific SSTs and anti-correlated with eastern Pacific and eastern Indian Ocean SSTs (Fig. 4a). The spatial pattern is similar to that for Malaysian rainfall (Tangang and Juneng 2004), which suggests the influences on rainfall for Singapore and for Malaysia are similar during this season.

The ENSO signal is evident during JJA (Fig. 4b) and SON (Fig. 4c), albeit weaker in the latter. Similarly, the correlations of SgP03 with SSTs in the Maritime Continent peak in JJA before weakening in SON. On the other hand, the correlation of SgP03 with western Indian Ocean SST strengthens from JJA to SON. The SgP03–SST correlation maps in JJA and SON are similar to those for Indonesian rainfall (Hendon 2003).

An abrupt change occurs in DJF as SgP03–SST correlations throughout the equatorial Indo-Pacific drop to non-significant values (Fig. 4d). This drop was also observed for Indonesian rainfall (Hendon 2003). The corresponding correlation map for OND (not shown) indicates that the collapse in correlation coefficients occurs up to two months earlier, following the end of the

Southwest Monsoon and during the inter-monsoon months of October and November. The SgP03–SST correlation map stands in stark contrast with the corresponding map for Malaysian rainfall (Tangang and Juneng 2004), in which the correlations between Malaysian rainfall and local/remote SSTs peak in DJF.

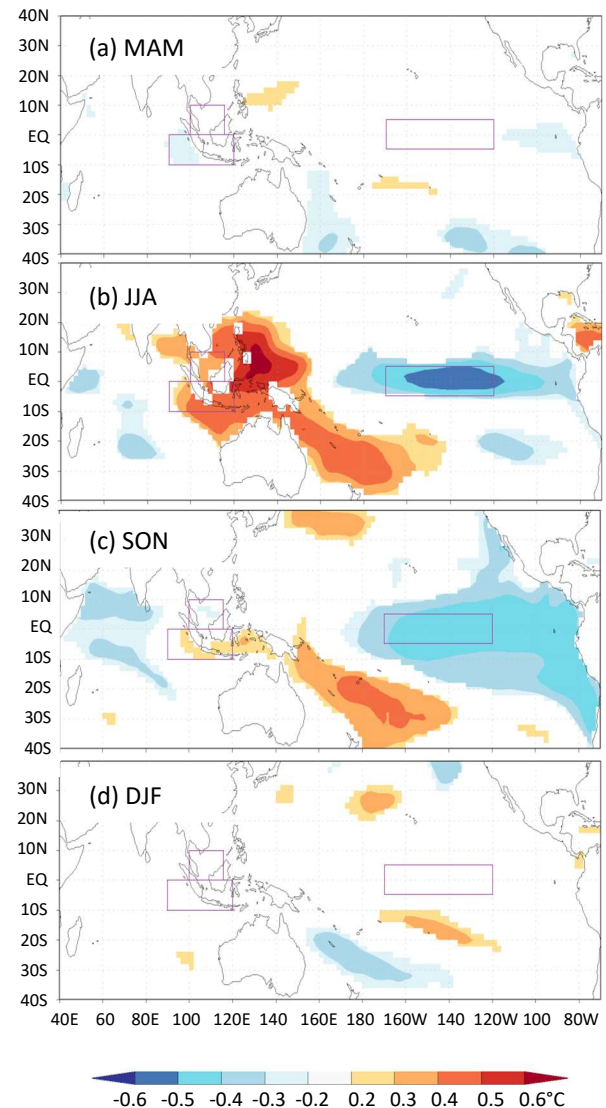


Figure 4. Simultaneous correlation between SgP03 and SST for (a) March–May, MAM, (b) June–August, JJA, (c) September–November, SON and (d) December–February, DJF, based on detrended data from Sep 1956 to Aug 2016. Correlation coefficients with p-values > 0.1 are not plotted. The boxes demarcate the three oceanic regions underlying the SST indices.

MONTHLY CORRELATIONS OF SGP03 WITH SST INDICES

As ENSO exerts a strong influence on both local SSTs and Singapore rainfall, we first investigate the

correlations between Nino3.4 and local SST indices. From Fig. 5, IndoSST is significantly correlated with Nino3.4 from December through May and significantly anti-correlated from August through October, whereas ScsSST is significantly correlated with Nino3.4 from November through June. Hendon (2003) showed that the changes in the sign of the correlation between central equatorial Pacific and Indonesian SSTs can be attributed to the evolution of wind speed and surface shortwave radiation anomalies as ENSO events mature.

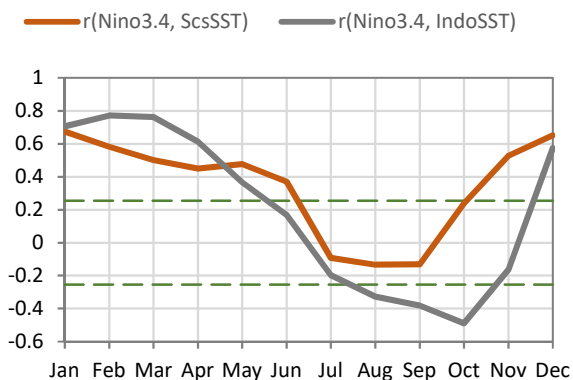


Figure 5. Simultaneous correlation coefficients between Nino3.4 and the local SST indices used in this study, based on detrended data from Sep 1956 to Aug 2016. Dashed horizontal lines indicate 95% significance level.

Assessing the relationship between SgP03 and Nino3.4 (Fig. 6a), the two variables are significantly anti-correlated from June through October. This characteristic is also true of Indonesian rainfall (Hendon 2003) and Malaysian rainfall (Tangang and Juneng 2004), which suggests that ENSO exerts a large-scale spatially coherent impact on rainfall over the much of the Maritime Continent during this period.

After controlling for the influence of IndoSST, we find that the partial correlation between SgP03 and Nino3.4 (dotted line, Fig. 6a) is considerably weaker and non-significant in August through October. This weaker correlation suggests that, as Hendon (2003) postulated for Indonesian rainfall, the cool (warm) SST anomalies induced by El Niño (La Niña) around Indonesia in Fig. 5 reinforce the large-scale ENSO impact on rainfall over Singapore during this period.

The correlation between SgP03 and Nino3.4 becomes insignificant by November and changes sign in December (Fig. 6a). The correlation is near zero in January and February. This evolution in the SgP03–Nino3.4 relationship explains the sudden collapse in seasonal correlation coefficients from SON to DJF (Fig. 4).

In contrast, the anti-correlation between Malaysian rainfall and Nino3.4 remains significant through boreal summer to March (Tangang and Juneng 2004).

There is a near-significant anti-correlation between SgP03 and Nino3.4 in March, with a smaller magnitude in April (Fig. 6a). It should be noted, however, that the correlation collapses when the influence of IndoSST is removed. This collapse suggests that the ENSO influence on local rainfall is strongly mediated by SST anomalies in the seas around Indonesia in March and April, as in ASO. The mechanism, however, is different, given that IndoSST anomalies tend to follow those in the Niño 3.4 region in March and April (Fig. 5).

In May, an abrupt reversal in the relationship between SgP03 and Nino3.4 to a near-significant positive correlation is observed. This reversal is not seen in Indonesian nor Malaysian rainfall (Hendon 2003; Tangang and Juneng 2004). The similarity between MAM and OND in terms of the evolution of the correlation coefficient suggests that the phenomenon may be related to the passing of the ITCZ over Singapore and the ensuing change in the background flows.

The SgP03–Nino3.4 correlation changes sign again between May and June (Fig. 6a). Notably, the ENSO forcing on rainfall over Singapore, with the influence of local SSTs removed, is stronger in June than at any other time of the year.

Shifting the focus from SgP03–Nino3.4 to SgP03–IndoSST, there is a significant correlation between SgP03 and IndoSST from July through October (Fig. 6b), due in part to ENSO's influence on both variables, as the warm (cool) phase of ENSO sees cool (warm) anomalies in the seas around Indonesia from July through October (Fig. 5) and, concurrently, suppressed (enhanced) rainfall over Singapore (Fig. 6a). With the influence of Nino3.4 removed, the SgP03–IndoSST relationship is noticeably weaker, particularly in October. The opposite is true in June, when IndoSST and Nino3.4 anomalies tend to have the same sign.

During the Southwest Monsoon, the SgP03–IndoSST partial correlation (grey dotted line, Fig. 6b) is significant (or nearly so). Thus, for any given ENSO phase, positive (negative) rainfall anomalies over Singapore during Jun-Sep are associated with warm (cold) anomalies in the Indonesian seas south of Singapore, presumably due to positive (negative) moisture anomalies in the south-southwesterly monsoon winds during this season.

Rainfall over Singapore during the Southwest Monsoon is also correlated with ScsSST (Fig. 6b). With the influence of Nino3.4 removed, the SgP03–ScsSST correlation is significant (or nearly so) in June-

September. Given that the prevailing winds over Singapore are south-southwest during this season, the impact of ScsSST on local rainfall is possibly through its influence on the background monsoon winds rather than due to its effect on atmospheric moisture.

The SgP03–ScsSST relationship is significantly modulated by ENSO in June, with the total correlation being much smaller than the partial correlation removing Nino3.4 (Fig. 6b). During the warm (cool) ENSO phase, the South China Sea is warmer (cooler) than normal in June, unlike JAS (Fig. 5), while rainfall over Singapore is suppressed (enhanced; Fig. 6a). As a result, the relatively strong SgP03–ScsSST relationship (removing Nino3.4) in June is masked by the ENSO influence on both variables.

In the inter-monsoon period (October and November), the relationship between SgP03 and IndoSST, removing Nino3.4, is much weaker than during June to September (Fig. 6b), possibly as a consequence of reduced winds from the south-southwest. Concurrently, there is an abrupt reversal of the SgP03–ScsSST relationship. The reasons for this reversal are not apparent, but the timing suggests it is also associated with the cessation of the Southwest Monsoon. The following season (DJF) sees very little correlation between SgP03 and the local SST indices.

There is a significant or near-significant anti-correlation between SgP03 and IndoSST in March and April (Fig. 6b), which indicates that rainfall over Singapore decreases (increases) when the Indonesian seas are warmer (cooler) than normal. This counter-intuitive relationship may be attributed to ENSO. As Fig. 5 shows, the IndoSST–Nino3.4 correlation is very strong in March; SST anomalies around Indonesia tend to follow

those in the central equatorial Pacific. At the same time, there is a near-significant anti-correlation between SgP03 and Nino3.4. The net result appears to be a relatively strong SgP03–IndoSST anti-correlation. If the influence of ENSO is removed, the relationship between rainfall over Singapore and Indonesian SSTs becomes much weaker, as indicated by the partial correlation between SgP03 and IndoSST (Fig. 6b).

During March and April, while ENSO strengthens the apparent SgP03–IndoSST relationship, it masks that between rainfall over Singapore and ScsSST. Although the relationship is non-significant, the partial correlation of SgP03 with ScsSST given Nino3.4 indicates that rainfall over Singapore in March and April tends to be higher (lower) whenever the South China Sea is anomalously warm (cool) irrespective of the state of the central equatorial Pacific (Fig. 6b).

In May, the SgP03–IndoSST correlation switches abruptly to positive (Fig. 6b) in connection with a similar change in the SgP03–Nino3.4 relationship (Fig. 6a), as Indonesian SST anomalies continue to follow those in the Niño 3.4 region (Fig. 5). At the same time, the correlation between SgP03 and ScsSST strengthens to near-significant levels. The corresponding partial correlations are smaller, indicating that ENSO’s influence on both rainfall (Fig. 6a) and local SSTs (Fig. 5) is an important factor in the apparent strength of the relationships.

GENERAL DISCUSSION

It is beyond the scope of this study to investigate the atmospheric and oceanic processes that produce the observed SgP03–SST correlations and their evolution

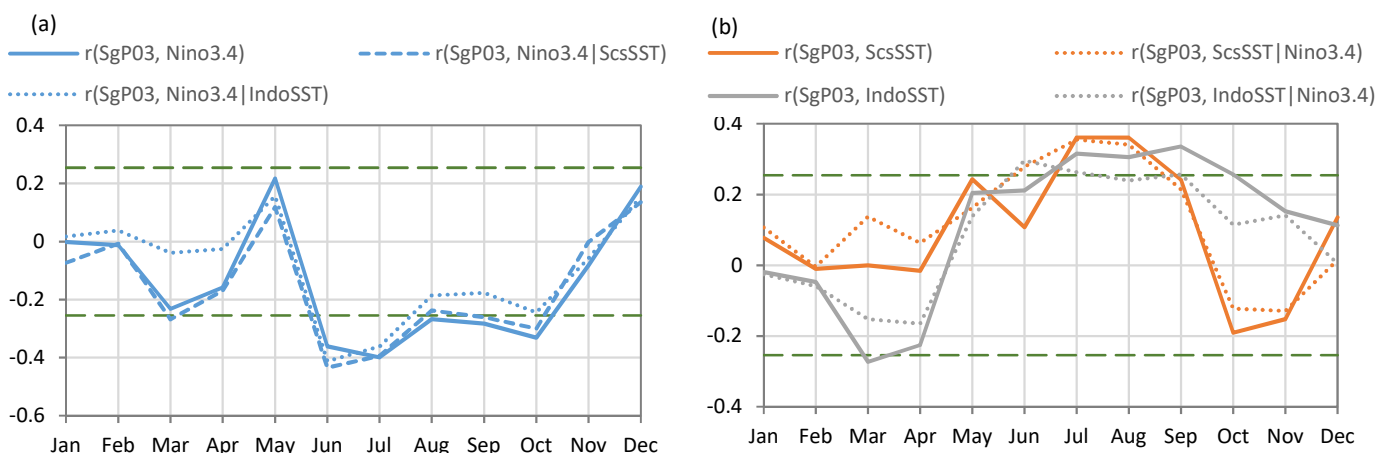


Figure 6. Simultaneous correlation coefficients between SgP03 and the SST indices used in this study, based on detrended data from Sep 1956 to Aug 2016. Total (partial) correlations are shown as solid (dotted and dashed) lines. Legend label $r(\text{SgP03}, \text{SST1})$ denotes correlation between SgP03 and SST1, whereas $r(\text{SgP03}, \text{SST1} | \text{SST2})$ denotes partial correlation between SgP03 and SST1, with the influence of SST2 removed. Dashed horizontal lines indicate the 95% significance level.

through time, but we shall briefly review the hypotheses that have been proposed.

The weakening (strengthening) of the Walker Circulation that is associated with El Niño (La Niña) induces SST anomalies of opposite signs in the western and central-eastern equatorial Pacific. In JJA and SON, the SST anomaly in the western equatorial Pacific extends to the waters around western Indonesia (Hendon 2003). Hendon (2003) postulates that the cool (warm) anomaly that develops in the waters around Indonesia during JJA and SON due to El Niño (La Niña) reinforces the large-scale impact on Indonesian rainfall, resulting in a strong and spatially coherent signal in this period. This study supports this hypothesis.

Between November and December, there is an abrupt switch in the sign of IndoSST with respect to Nino3.4 (Fig. 5). Hendon (2003) argues on this basis that the weak rainfall–SST correlations observed during DJF are due to the opposing effects of ENSO and local SSTs on Indonesian rainfall. This hypothesis does not appear to hold for Singapore. If warm (cool) local SSTs counterbalanced the influence of El Niño (La Niña) on local rainfall during DJF, we should observe positive partial correlations between rainfall and local SSTs larger than the corresponding total correlations. On the contrary, for December, where we observe the strongest rainfall–SST correlations in the season, the partial correlations are uniformly smaller than the corresponding total correlations (Fig. 6). This implies that SST anomalies in the local and remote regions support rather than counterbalance one another in their relationships with rainfall over Singapore. Similar arguments led Tangang and Juneng (2004) to conclude that ENSO-driven local wind anomalies rather than local SSTs are the main factor for the observed anti-correlation between Malaysian rainfall and Nino3.4 in DJF.

CONCLUSION

This study investigated the variability of seasonal and monthly rainfall over Singapore from 1956–2016 in relation to SSTs in the western Maritime Continent and the central equatorial Pacific. A few key findings emerge from the correlation analyses.

There is a strong ENSO forcing on rainfall over Singapore from June through October, consistent with the large-scale effects on the western Maritime Continent. Although the ENSO influence on other seasons was not significant, rainfall over Singapore tends to be higher (lower) in May and December, and lower (higher) in March, during El Niño (La Niña).

ENSO's influence on rainfall over Singapore is to a significant degree contingent on associated SST anomalies around Indonesia. As such, the state of the Indonesian seas has to be considered in making sub-seasonal to seasonal predictions of rainfall over Singapore during El Niño or La Niña. If Indonesian SSTs fail to respond to SST anomalies in the central equatorial Pacific in the way they typically do, a muted rainfall response may be expected.

While ENSO's impact on rainfall over Singapore is largely independent of the state of the South China Sea, there is a significant correlation between rainfall over Singapore and SST in the South China Sea during JJA, independent of ENSO. This correlation implies that variability in the JJA rainfall among years with the same ENSO phase can be attributed partly to the state of the South China Sea. As such, the latter provides useful information— independent of central equatorial Pacific SSTs—for sub-seasonal to seasonal rainfall forecasts for Singapore.

Local SSTs are not the only or even the main factors behind the rainfall anomalies observed in this region. The contrasting evolution of Malaysian rainfall (aggregated based on stations north of the Equator) and Indonesian rainfall (based largely on stations south of the Equator) suggests that the background monsoon flow, which changes direction over the Equator, plays an important role in modulating the effect of ENSO on the western Maritime Continent. This relationship will be investigated in a subsequent paper.

REFERENCES

- Chang, C.P., Wang, Z., Ju, J., and Li, T. (2004) On the Relationship between Western Maritime Continent Monsoon Rainfall and ENSO during Northern Winter. *Journal of Climate*, 17:665–672.
- Cheong, W.K. (2013) Statistical relationships between ENSO and climate over Singapore. Meteorological Service Singapore Knowledge Sharing Session, Singapore.
- Hendon, H.H. (2003) Indonesian Rainfall Variability: Impacts of ENSO and Local Air–Sea Interaction. *Journal of Climate*, 16:1775–1790.
- Huang, B., Thorne, P.W., Banzon, V.F., Boyer, T., Chepurin, G., Lawrimore, J.H., Menne, M.J., Smith, T.M., Vose, R.S., and Zhang, H.M. (2017) Extended Reconstructed Sea Surface Temperature, Version 5 (ERSSTv5): Upgrades, Validations, and Intercomparisons. *Journal of Climate*, 30:8179–8205.

KNMI (2018) The KNMI Climate Explorer. Available at: <https://climexp.knmi.nl>, last accessed: 3 January 2018.

McBride, J.L., Haylock, M.R., and Nichols, N. (2003) Relationships between the Maritime Continent Heat Source and the El Niño–Southern Oscillation Phenomenon. *Journal of Climate*, 16:2905–2914.

NOAA (2018) Climate Prediction Center – ONI. Available at: http://origin.cpc.ncep.noaa.gov/products/analysis_mon/ito_ring/ensostuff/ONI_v5.php, last accessed: 3 January 2018.

Ropelewski, C.F., and Halpert, M.S. (1987) Global and Regional Scale Precipitation Patterns Associated with the El Niño/Southern Oscillation. *Monthly Weather Review*, 115:1606–1626.

Tangang, F.T. and Juneng, L. (2004) Mechanisms of Malaysian Rainfall Anomalies. *Journal of Climate*, 17:3616–3622.

WIND ANOMALIES OVER SINGAPORE AND THE SURROUNDING REGION

Synoptic scale drivers during the Southwest Monsoon

Cheong Wee Kiong and Zheng Kaiyuan

Weather Services Department, Meteorological Service Singapore

INTRODUCTION

The Southeast Asian region experiences two major monsoon seasons, the Southwest (SW) and Northeast (NE) Monsoons, driven by the annual march of the tropical rain belt known as the Inter-Tropical Convergence Zone (ITCZ). The SW Monsoon occurs when the ITCZ is in the northern hemisphere, typically from June to September. This monsoon period is drier in the southern Southeast Asia region compared to the NE Monsoon and the most likely time of the year for haze in Singapore.

Over Singapore and the surrounding region, the prevailing SW Monsoon winds typically blow from the southeast or southwest (Chang, 2005) especially during August to October (Fig. 1 left). Nevertheless, there are noticeable deviations from this mean climatological pattern, such as in Aug–Oct 2016 when winds had an anomalous west to northwest component (Fig. 1 right). An increase in westerlies during these months is noteworthy. Stronger westerlies could alter the rainfall

thereby affecting spatial and temporal patterns of haze conditions for Southeast Asia, and consequently modulating the air quality for Singapore and the surrounding region. Therefore, improved characterisation of these wind anomalies and understanding the mechanisms behind their formation would help anticipate regional changes in wind patterns and their consequences.

There have been a variety of studies concerning rainfall in the region and its large-scale drivers. El Niño Southern Oscillation (ENSO) is a well-known important driver of rainfall variability in the equatorial Pacific region (Aldrian and Dwi Susanto 2003; Dobles-Reyes et al. 2013). Several other studies suggest that large-scale rainfall patterns in this region are also affected by other major weather systems such as the Indian Ocean Dipole (IOD) and the Madden Julian Oscillation (MJO; Reid et al. 2012; Dobles-Reyes et al. 2013). However, none of these studies has considered the direct impacts of such large-scale drivers to the wind conditions over Singapore and the surrounding region.

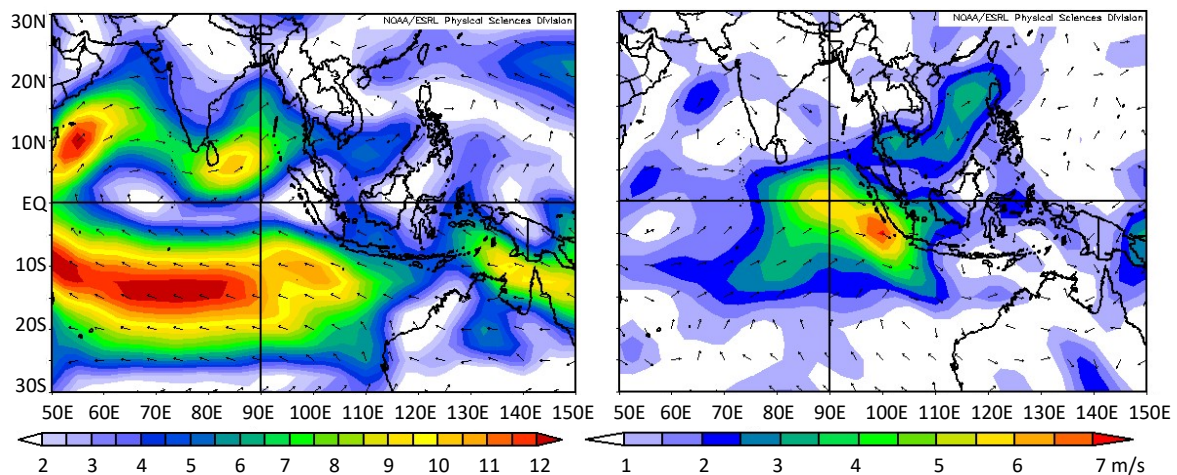


Figure 1. Long-term mean wind field at 925 hPa, surrounding Singapore, averaged over August, September and October computed from 1981 to 2010 (left); wind directions are shown with arrows while colour background indicates wind speed. The right panel shows the anomalies for the same quantity from the long-term mean for the year 2016. The plots were constructed using the NCEP/NCAR Reanalysis data (Kalnay et al. 1996).

Therefore, this study aims to investigate the potential influence of these well-known synoptic scale phenomena to the wind anomalies over the region during the SW Monsoon.

DATA AND METHODOLOGY

Wind data were extracted from the NCEP reanalyses, derived from the joint efforts of the National Centres for Environmental Prediction (NCEP) and National Centre for Atmospheric Research (NCAR) in their “40-year Reanalysis Project” (Kalnay et al. 1996). The Earth System Research Laboratory, Physical Sciences Division from the National Oceanic and Atmospheric Administration (NOAA) publicly make available this reanalysis data on their website, which also serves as a platform that allows users to plot composite charts of their parameters and timescales of interest (NOAA 2017).

The commonly used all-season Real-time Multivariate MJO index (RMM; Wheeler and Hendon 2004) are used to monitor the location and strength of the MJO and were retrieved from the Bureau of Meteorology, Australia (BOM, 2017). State of the IOD is monitored using the Dipole Mode Index (DMI; Saji et al. 1999), retrieved from the Japan Agency For Marine-Earth Science And Technology (JAMSTEC 2017). ENSO status is monitored using the sea surface temperature anomalies within the Niño 3.4 region (Trenberth 1997) obtained from the National Weather Service, Climate Prediction Centre (CPC 2017).

Long-term (1981–2010) composites of winds at the 1000 hPa, 925 hPa, 850 hPa and 700 hPa levels over the domain of 30°N, 30°S, 50°E, 130°E during August, September, and October were generated in order to determine the typical wind conditions over Singapore and the surrounding region. These levels were selected based on experience from operational forecasting on which levels influence the weather and air quality conditions significantly over Southeast Asia.

Composite maps for westerly-northwesterly (W-NW) as well as southeasterly-easterly (SE-E) monthly wind anomalies were computed by first calculating the monthly wind anomalies for August, September, and October from 1980 to 2016. The individual months of those years with either SE-E anomalies or W-NW anomalies were selected based on the approximate region 5°N, 5°S, 80°E, 100°E. A month was deemed anomalous if the average anomaly in the region was at least 1.5 m/s, with a westerly component (W-NW anomaly) or easterly component (SE-E anomaly). As the months were analysed separately, it is possible only one

month was selected for any particular year. The wind from selected years for each month and group (SE-E and W-NW anomalies) were then averaged and the final composites of wind anomalies were generated by subtracting the average wind in the SE-E and W-NW anomaly groups from the long-term (1981–2010) mean wind. In order to identify which synoptic scale drivers played a more significant role in modulating the anomalous regional wind condition, the corresponding MJO, DMI, and Niño3.4 indices for each year and month when wind anomaly was observed were determined.

In addition, composite maps were constructed based on the state of the IOD: all positive, negative, and neutral events. An event was classified as positive (negative) if the DMI > 0.4 (< -0.4).

RESULTS

The composite maps for August, September, and October show wind anomalies at the 925 hPa level, which stretches from the equatorial Indian Ocean to Singapore and the surrounding region, for both the SE–E (Fig. 2. left) and W–NW anomalies (Fig. 2 right). The main wind anomalies are over the Indian Ocean off the western coast of Sumatra based on the selection criteria, although anomalies can also be observed over Australia during August and September, as well as the South China Sea (all months). Similar anomalous wind conditions are also apparent at the 1000 hPa, 850 hPa and 700 hPa levels (not shown), indicating deep anomalies not confined to the surface.

The potential influence of large modes on naturally occurring variability (ENSO and IOD) on the wind anomalies depicted by these composites are analysed by looking at the values of the indices for these modes of variability (DMI, Niño3.4, respectively) for August, September, and October (Table 1). For the other mode of variability, MJO, Table 1 includes the observed number of days of occurrence for each of the MJO phases, where days with a magnitude less than one were considered to be weak. The average number of occurrences for MJO phase, mean DMI, and mean Niño3.4 values for W-NW and SE-E anomalies are also included in the table along the top rows of each regime.

While weak MJO conditions prevailed in Table 1 regardless of the direction of the wind anomalies, the more frequent occurrence of MJO in phases 5 to 8 tends to favour W-NW wind anomalies (on average, 10.5 days per month). However, it is not uncommon for SE-E wind anomalies also to occur under such MJO conditions (average 5.3 days per month). During August and October, the occurrence of MJO in phases 1 and 2 tends

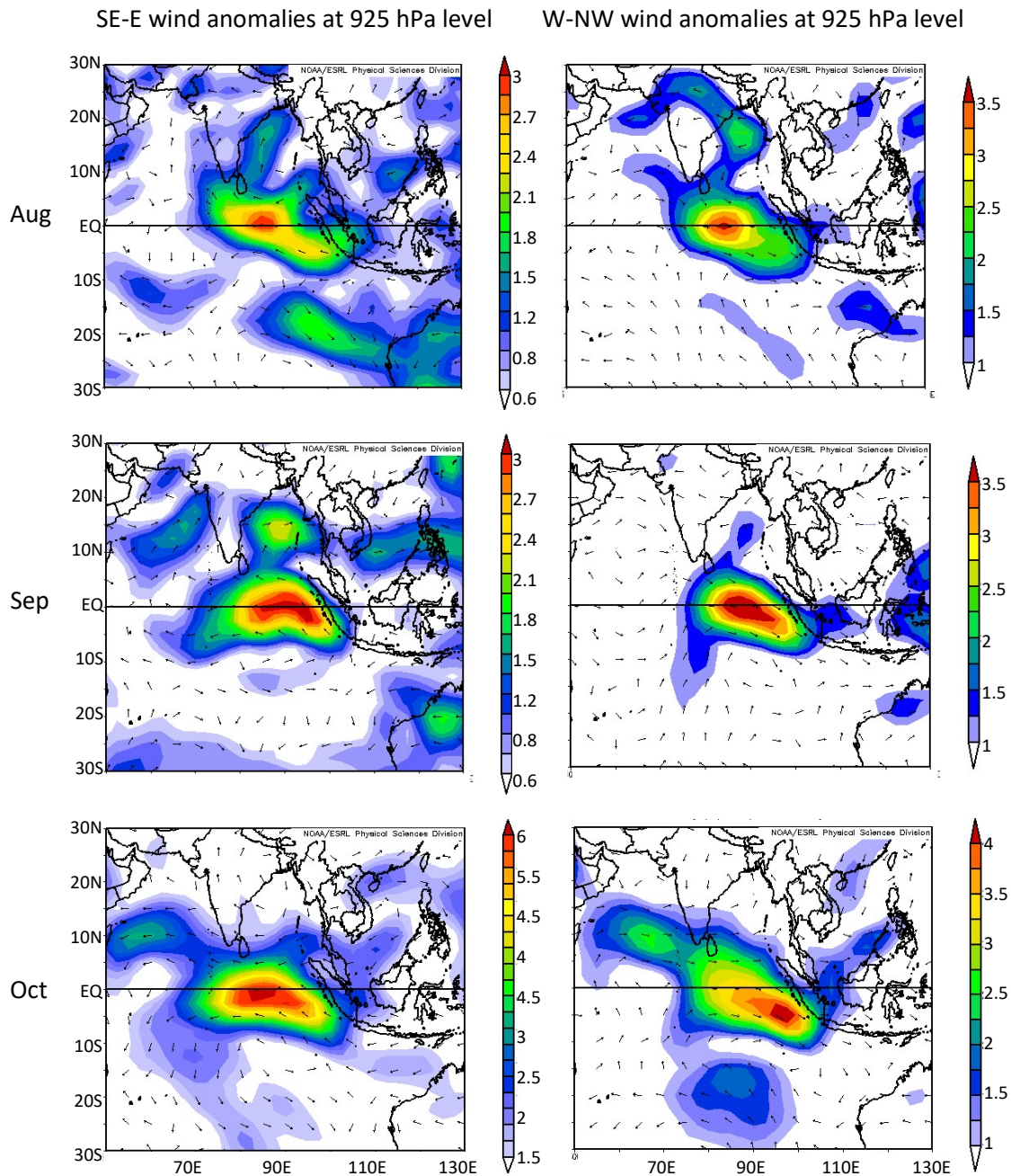


Figure 2. Same as Figure 1 but for the composites of easterly to southeasterly anomalies (left panel) and westerly to west-northwesterly anomalies (right panel) at the 925 hPa level for August (top row), September (middle row) and October (last row) in years with the respective dominant flows. Anomalies are in m/s.

to favour SE-E wind anomalies (average 7.5 days per month), although these phases have also been observed with W-NW wind anomalies (average 1.7 days per month). Therefore, these results suggest that MJO phases are not a strong determinant of the monthly regional wind anomalies during the SW Monsoon.

Similarly, there is a mixed signal from ENSO conditions on the wind anomalies. La Niña seems to be favourable for the W-NW wind anomalies; Nino3.4 values are mostly negative with four months out of six in August, all months in September and October, and many values are below than -0.5 the threshold for La

Niña conditions. Nevertheless, in some instances, La Niña conditions are also present in three occurrences of the SE-E wind anomalies in September. However, SE-E wind anomalies are predominantly observed with Nino3.4 positive values (all cases in August, and October and half the cases in September) many being above the El Niño threshold (average Nino3.4 value is 0.59). On face value, these results suggest that ENSO is possibly an important large-scale driver contributing to the wind anomalies. SE-E anomalies in October are not only associated with positive Nino3.4 values; these months also record positive DMI values.

		W-NW Anomalies						
	Year	IOD	ENSO	MJO phases				
		DMI	Nino3.4	1&2	3&4	5&6	7&8	Weak
W-NW mean		-0.60	-0.48	1.7	3.1	7.1	3.4	15.3
August	1989	-0.64	-0.31	0	0	1	2	28
	1990	-0.20	0.34	0	0	11	1	19
	1992	-0.57	0.15	0	0	7	0	24
	1996	-0.89	-0.17	6	8	2	0	15
	2010	-0.45	-1.22	4	0	5	0	22
	2016	-0.65	-0.63	0	0	16	1	14
September	1984	-0.29	-0.21	0	0	1	14	15
	1992	-0.89	-0.04	4	0	4	11	11
	1995	0.07	-0.79	0	1	14	0	15
	1996	-0.37	-0.38	0	0	13	4	13
	1998	-0.78	-1.13	0	11	2	10	7
	2005	-0.59	-0.03	0	7	10	5	8
	2010	-0.87	-1.48	8	1	0	0	21
	2016	-0.97	-0.62	0	7	10	0	13
October	1984	-0.16	-0.47	0	0	3	17	11
	1992	-0.50	-0.21	0	10	11	2	8
	1996	-1.13	-0.35	4	2	2	1	22
	1998	-0.91	-1.27	0	0	16	0	15
	2005	-0.30	-0.1	8	8	4	0	11
	2016	-0.98	-0.62	0	7	10	0	14
			SE-E Anomalies					
SE-E mean		1.06	0.59	7.5	5.8	3.3	2.0	12.0
August	1983	0.45	0.02	2	16	0	0	13
	1987	0.20	1.64	11	16	4	0	0
	1994	1.62	0.48	7	0	0	0	24
	2012	1.05	0.23	14	9	2	1	5
September	1987	0.64	1.66	6	11	4	0	9
	1994	1.46	0.24	0	0	7	14	9
	1999	0.13	-0.99	12	0	0	1	17
	2006	1.33	0.52	4	19	2	0	5
	2007	0.92	-0.93	3	1	17	0	9
	2011	0.91	-0.86	0	4	6	0	20
October	1982	0.77	2.01	11	1	0	0	19
	1991	0.74	0.82	9	10	0	2	10
	1994	2.34	0.57	21	4	0	2	4
	1997	2.27	2.24	6	0	0	3	22
	2002	0.66	1.1	6	2	3	0	20
	2006	1.54	0.63	8	0	8	9	6

Table 1. Selected months with westerly-northwesterly wind anomalies (W-NW, top) and southeasterly to easterly wind anomalies (SE-E, bottom). For each month, the monthly DMI and Nino3.4 values are calculated, as well as the number of days of each set of MJO phases (days with amplitudes less than one were classified weak). Highlighted in blue are the years with negative IOD phases and orange are the years with positives IOD phases.

The characteristics of the two directions of wind anomalies become more distinct when considering the IOD phase. The average DMI value for all anomalous months is -0.60 and 1.06 for W-NW and SE-E anomalies, respectively. Furthermore, out of the 20 occurrences of W-NW wind anomalies, 13 occur during the negative phase of the IOD (highlighted in blue, Table 1). Out of the 16 occurrences of SE-E wind anomalies, 13 of them were during the positive phase of the IOD. For the remainder of both directional anomalies, the IOD status was neutral. With a high proportion of W-NW wind anomalies (SE-E wind anomalies) events during negative (positive) IOD phase, it suggests that the different phases of IOD play a major role in modulating the regional wind conditions.

The importance of the IOD in driving these wind anomalies is further evaluated by plotting the composites of negative (positive) IOD years and showing the difference between the two (Fig. 3). General wind anomalies are reminiscent of what was observed on the composite constructed based on wind

anomalies. The difference between the two composites suggests that the impact of negative IOD phase in inducing the W-NW wind anomalies is stronger than the impact of positive IOD phase in bringing the SE-E wind anomalies over Singapore and the surrounding region. Similar results can be observed from the 850 hPa and 700 hPa pressure levels (not shown). Additional analysis on the impacts of IOD to monthly rainfall (Heng and Gao, 2018) found that Singapore will generally be wetter-than-normal (drier-than-normal) during positive (negative) IOD years for the SW Monsoon season, supporting that IOD modulates weather systems in the region.

CONCLUSION

Over Singapore and the surrounding region, the prevailing low-level SW Monsoon winds typically blow from the southeast or southwest. However, there have been noticeable deviations from this mean climatological wind pattern, such as an anomalous west

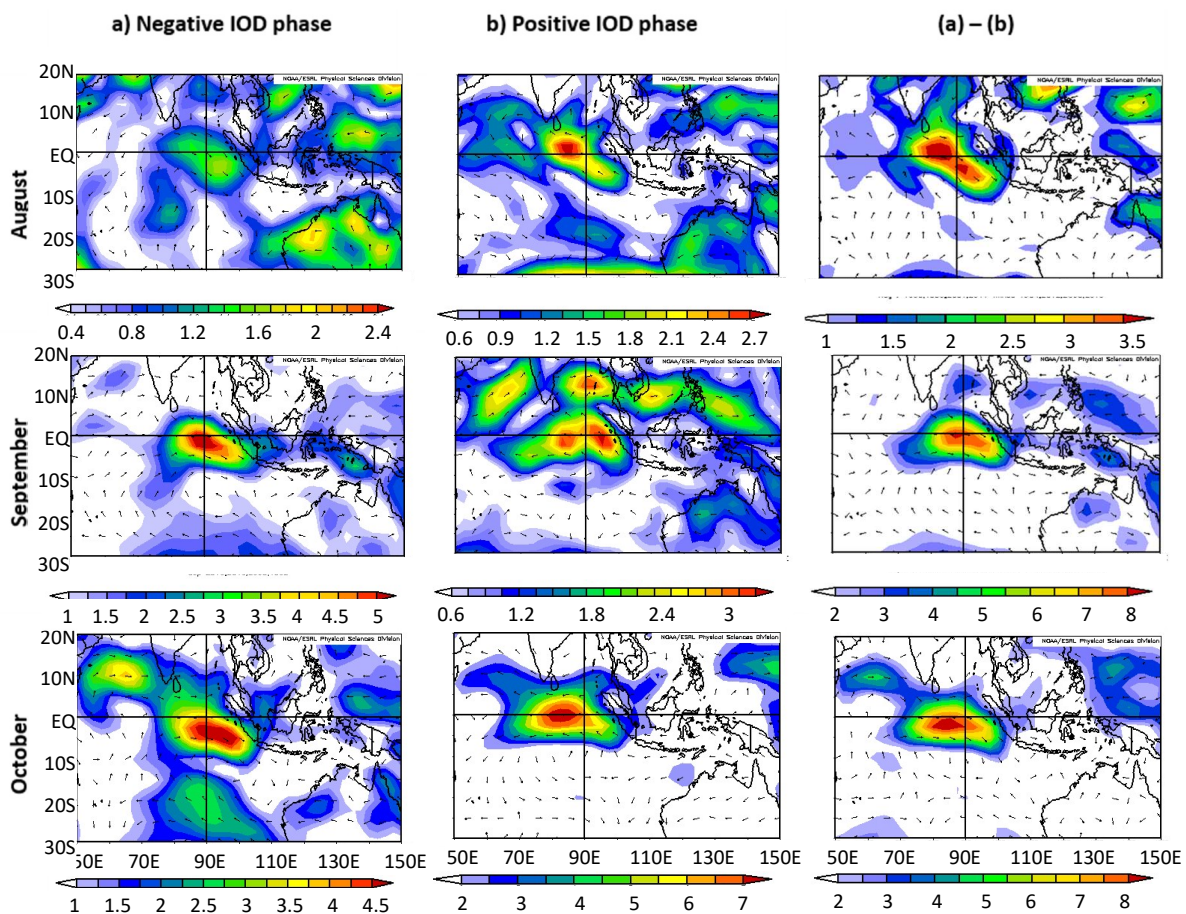


Figure 3. Mean wind field at 925 hPa, August (top row), September (middle row) and October (last row) in a) Negative IOD phase (left panel), b) Positive IOD phase (middle panel) and difference of the composite wind during negative IOD years and the composite wind during positive IOD years (right panel). The wind anomalies are in m/s.

to northwest component in 2016. Several studies have indicated that ENSO, IOD, and MJO are major drivers of rainfall variability in the equatorial Pacific region. However, few of these studies considered directly the impacts of such large-scale drivers to the wind conditions over the region surrounding Singapore. This study investigated the potential influence of these well-known synoptic scale phenomena to the wind anomalies over the region during August, September, and October. NCEP reanalysis wind data was used to identify years with SE-E wind anomalies and W-NW wind anomalies between 1980 and 2016 for the months August, September, and October during the SW Monsoon. While the frequent occurrence of MJO phases 1 and 2 tended to favour SE-E wind anomalies during August and October, MJO and ENSO were unlikely the key synoptic drivers contributing to the monthly wind anomalies over Singapore and the surrounding region. Despite the link between IOD events and some ENSO events (particularly for October), IOD likely played a more significant role compared to the others in modulating the regional wind conditions during these months; bringing W-NW wind anomalies (SE-E wind anomalies) during the negative (positive) IOD phase. The results from this study, therefore, suggest that IOD is playing a significant role in modulating the wind and weather conditions over the region surrounding Singapore. It would be useful to continue this work by looking into the direct impacts of such large-scale drivers to the regional haze episodes. Furthermore, the approach used here may be useful for other seasons and regions in Southeast Asia.

REFERENCES

- Aldrian, E. and Dwi Susanto, R. (2003) Identification of three dominant rainfall regions within Indonesia and their relationship to sea surface temperature. *International Journal of Climatology*, 23:1435–1452.
- BOM (2017) MJO RMM index. Available at: <http://www.bom.gov.au/climate/mjo/graphics/rmm.74toRealtime.txt>, last accessed: 28 March 2018.
- Chang, C.P. (2005) The Maritime Continent Monsoon. In *The Global Monsoon System: Research and Forecast* Ed. Chang, C. P., Wang, B., Lau, N. C. G., WMO, 156–178.
- CPC (2017) Nino3.4 index. Available at: <http://www.cpc.ncep.noaa.gov/data/indices/>, last accessed: 28 March 2018.
- Doblas-Reyes, F.J., García-Serrano, J., Lienert, F., Biescas, A.P., and Rodrigues, L.R.L. (2013) Seasonal climate predictability and forecasting: status and prospects. *WIREs Climate Change*, 4:245–268.
- Heng, B.C.P. and Gao, E. (2018) Rainfall over Singapore in relation to local and remote sea surface temperatures. *MSS Research Letters*, 1:14–19.
- JAMSTEC (2017) Dipole Mode Index. Available at: http://www.jamstec.go.jp/frsgc/research/d1/iod/e/iod/dipole_mode_index.html, last accessed: 28 March 2018.
- Kalnay, E., Kanamitsu, M., Kistler, R., Collins, W., Deaven, D., Gadin, L., Iredell, M., Saha, S., White, G., Woollen, J. et al. (1996) The NCEP/NCAR 40-year Reanalysis Project. *Bulletin of the American Meteorological Society*, 77:437–472.
- NOAA (2017) NCEP reanalysis data. Available at: <https://www.esrl.noaa.gov/psd/>, last accessed: 28 March 2018.
- Reid, J.S., Xian, P., Hyer, E.J., Flatau, M.K., Ramirez, E.M., Turk, F.J., Sampson, C.R., Zhang, C., Fukada, E.M., and Maloney, E.D. (2012) Multi-scale meteorological conceptual analysis of observed active fire hotspot activity and smoke optical depth in the Maritime Continent. *Atmospheric Chemistry and Physics*, 12:2117–2147.
- Saji, N.H., Goswami, B.N., Vinayachandran, P.N., and Yamagata, T. (1999) A dipole mode in the Indian Ocean. *Nature*, 401:360–363.
- Trenberth, K.E. (1997) The Definition of El Niño. *Bulletin of the American Meteorological Society*, 78:2771–2778.
- Wheeler, M.C. and Hendon, H.H. (2004) An All-Season Real-Time Multivariate MJO Index: Development of an Index for Monitoring and Prediction. *Monthly Weather Review*, 132:1917–1932.

SINGAPORE AIR QUALITY: A HISTORICAL ANALYSIS

2010–2015

Eugene Chong Wei Ming

Applied Modelling Branch, Centre for Climate Research Singapore

INTRODUCTION

In 2011, the National Environment Agency (NEA) chaired an Advisory Committee comprising representatives from various governmental agencies and Institutes of Higher Learning, which provided a list of recommendations regarding Singapore's ambient air quality (NEA 2011). Subsequently, the Ministry of Environment and Water Resources (MEWR), together with the NEA, reviewed the recommendations of the Advisory Committee, as well as the Sustainable Singapore Blueprint to derive a revised set of National Air Quality targets pegged to World Health Organisation (WHO) Air Quality Guidelines. These revised targets have galvanised interest in identifying possible sources that impact local air quality and consequently our ability to achieve the targets.

Singapore's air quality is dependent not only on local emissions but also transport of pollutants from surrounding geographical regions. With rapid regional urbanisation and increased air/sea transportation, the impact of transboundary pollution is becoming increasingly important to local air quality. During transport from the source region, pollutants will mix and transform through various reactions. Pollutants may also be removed from the atmosphere by either gravitational fallout, surface entrainment, cloud droplets absorption, or precipitation washout. Therefore, information is needed on the background wind flow (for example, the output from a numerical weather prediction model; NWP), as well as a model to capture the spread of pollutants from the mean wind flow as well as the other interactions (termed a dispersion model). Dispersion models can be run in a forward mode to forecast dispersion from known emission sources, or backward mode to identify the likely geographical origin of particles from an observation point. Further information on atmospheric dispersion modelling can be found in Jones 2004.

The influence of different geographical areas in the region varies yearly as well as seasonally due to changing wind patterns. There are four wet/dry seasons

in Singapore: February, March, April (FMA), May, June July (MJJ), August, September, October (ASO), and November, December, January (NDJ). Large-scale modes of variability that affect the region include the El Niño Southern Oscillation (ENSO), Indian Ocean Dipole (IOD; Saji et al. 1999) and Madden-Julian Oscillation (MJO; Madden and Julian 1971). Conducting a multi-year analysis of the various seasons is, therefore, necessary to capture potential variability in pollutant source regions.

This study seeks to conduct an air history analysis to identify inter-annual and intra-annual variations in potential pollutant source regions and help explain vagaries in Singapore's air quality in recent years. Inverse or back trajectory analysis of airflow to Singapore was conducted using modelled PM10 particles as a tracer in a dispersion model. The study also assesses recent haze episodes for Singapore in 2013, 2014, and 2015.

METHODOLOGY

Since 2013, MSS has been collaborating with the UK Met Office (UKMO) to develop its in-house dispersion modelling capability. Dispersion modelling studies are conducted using the NAME dispersion model to aid in the understanding of transport and impact of windborne hazards on Singapore.

NAME DISPERSION MODEL

The Numerical Atmospheric dispersion Modelling Environment (NAME) model is a Lagrangian particle dispersion model developed by the UKMO for a range of hazards and pollution monitoring purposes (Jones 2004). A Lagrangian model like NAME simulates the dispersion by tracing the path of particles through a three-dimensional modelled space of the atmosphere. These particles drift and disperse along with the mean wind from NWP output or observed wind data over a certain time period. Movement of the particles is also driven by a random component to represent the effects of atmospheric turbulence.

The NAME model was conducted in inverse mode (termed 'backrun') for this study, whereby the run was conducted backwards in time using a particle tracer to locate possible pollutant originating sources. Modelled particles could be released into the atmosphere as a point source, line, area or geometrical shape such as a cuboid (rectangular), ellipsoid (circular) or cylindroid (circular in the horizontal, rectangular in the vertical). For this study, a cuboid emission source was used with dimensions 10 m by 10 m in the horizontal, with an emission depth of 10 m. The emission rate was set at an arbitrary unit of 1 g/s and emitted over 24 hours. The particles can represent pollutant particles with varying particulate sizes, radioactive particles, volcanic ash, or even different compounds and chemicals. In this case, the modelled particles were used to represent particulate matter less than 10 micrometres in diameter (PM10), which is an inert non-reactive pollutant.

UNIFIED MODEL

Global Unified Model (UM) output was used to conduct the backruns (Davies et al. 2005). The UKMO developed the UM as a seamless numerical atmospheric model designed to be used across various timescales and spatial scales. The UM fields provide sufficient resolution to determine the various geographical regions where air over Singapore originates while avoiding unnecessary granularity in resolving local variations in the wind fields, allowing for more efficient model runs over the long time period and large model domain. The Global UM data consist of 70 non-uniform vertical levels extending to an altitude of 80 km, with forecasts produced four times per day. For this study, a regional cut-out version of the Global UM data is used for the NAME backruns, which comprises 50–60 vertical levels from the surface up to an altitude of more than 20 km. This height is expected to be sufficient for the requirements of the NAME model runs, as the majority of pollution resides within the lowest 1–3 km of the atmosphere known as the planetary boundary layer (von Engel et al. 2013). The horizontal resolution of the UM data ranges from 17 to 40 km depending on the model version, as older versions of the UM are of lower resolution.

MODEL SETUP

To determine the potential pollutant source regions, NAME dispersion model backruns were driven using three-dimensional meteorology supplied by the Global UM. A large domain (23°N, 15°S, 90°E, 140°E)

around Singapore was chosen to assess how airflow originating from various parts of the region affect Singapore. The chosen boundaries include most of the major countries and cities in Southeast Asia, as well as major shipping lanes in the Straits of Malacca, Java Sea, and South China Sea, which are possible sources of emissions relevant to Singapore's air quality.

PM10 was used as a tracer and the backruns were conducted from a receptor site at Bishan. A test run between a coastal receptor site at Sentosa and an inland site at Bishan yielded insignificant variation, as the resolution of the UM global wind fields ranges from 17–40 km while Singapore only measures 50 km from east to west and 27 km from north to south. Wet and dry deposition are both turned on to simulate actual precipitation and gravitational settling scenarios during the modelled time periods. To allow sufficient time for transboundary particle transport, gravitational settling and deposition, a 10-days backrun was conducted for every single day in the time period 2010–2015 and concentration values in the 0–2 km layer were integrated at 10-minute time steps for the full duration of the run. The 0–2 km layer was chosen to represent the planetary boundary layer, where a majority of pollutants in the atmosphere reside, and the total integrated concentration was computed to provide an aggregated particle concentration value, indicative of the likelihood of pollutants originating sources. A percentile value was calculated to ascertain the likelihood of air originating from a particular geographical area compared to other areas. Percentiles are computed at 10% intervals by taking a fractional contribution of each grid point (0.1°) integrated concentration value as compared to the total integrated concentration present in the entire model domain.

The computations were conducted over a period of 6 years (2010–2015) to capture interannual variation in meteorological wind flow. The period between 2010 and 2015 includes a good mix of the various ENSO phases (El Niño, La Niña, and neutral events). It is expected that these six years are sufficient to provide an accurate depiction of long-term climatological air history and possible transport of pollutants from various geographical regions. Four periods were used, FMA, MJJ, ASO, and NDJ, to allow seasonal differences in pollutant source regions to be identified and provide a meteorological perspective on the causes for inter-year differences in air quality during certain seasons. The period also includes the most recent haze incidents that affected Singapore, including the dry spell in early 2014 and haze episodes in 2013, 2014, and 2015.

RESULTS

FULL TIME PERIOD ANALYSIS

When analysed across the full time period of the run (2010–2015), the percentiles of integrated particle concentrations from 2010 to 2015 (Fig. 1a) provides a geographical perspective on source regions for Singapore and shows a pattern similar to the climatological wind observations at Singapore Changi Climate station (Fig. 1b). Synoptic wind flow across the Southeast Asian region is primarily driven by the Asian Monsoon system. Owing to its geographical location near the equator, the dominant wind direction in Singapore during the Northeast Monsoon is from the northeast (more than 15% of counts in Fig. 1b) and from the southeast/south-southwest during the Southwest Monsoon (more than 15% of counts in Fig. 1b). The strong northeast/southeast wind directions are also seen in Fig. 1, with the 10th percentile values stretching as far northeast as the Philippines and as far southeast as East Timor.

On average, airflow over Singapore primarily originates over maritime regions like the South China Sea, Java Sea, and Malacca Strait as seen from the 50th percentile values. Land regions that are more significant source regions are southern coastal areas of Peninsular Malaysia (80–90th percentiles), Riau Islands (80th percentile), and eastern coastal areas of Sumatra. For Sumatra, the provinces of Riau, Jambi and South Sumatra are most significant airflow source regions (30–40th percentiles). Incidentally, these are also coastal peat-rich areas, which have been pollutant sources in the past. Kalimantan is also noteworthy as regions in the

southern coast of the island (10–20th percentile) have been the source of some pollution episodes in recent years. Other parts of Kalimantan are however less likely source areas for airflow over Singapore (below 10th percentile). Regions in northern ASEAN like Laos, Cambodia, and Thailand, the Philippines and the islands of Sulawesi and Papua New Guinea fall below the 10th percentile region, indicating that transboundary pollution over Singapore has a low likelihood of originating from there.

SEASONAL ANALYSIS

FEBRUARY-MARCH-APRIL (FMA)

FMA heralds the tail end of the dry season in the continental countries of Southeast Asia, such as Thailand, Cambodia, and Myanmar, with prolonged dry periods a common occurrence. The backrun maps for FMA show that these regions fall within the 10th percentile of source regions for Singapore (Fig. 2), indicating a low likelihood of pollutant sources originating from these regions. The primary area of concern to Singapore during this period would be southern Peninsular Malaysia, in particular areas in Johor to the northeast of Singapore such as Kota Tinggi and Pengerang, as well as maritime areas in the South China Sea to the northeast of Singapore. Maritime Southeast Asia (Indonesia) on the other hand experiences wetter conditions during these months, which help to suppress pollutant emissive events and transport.

Singapore experienced its longest recorded dry spell during FMA in 2014, including a stretch of 62 days

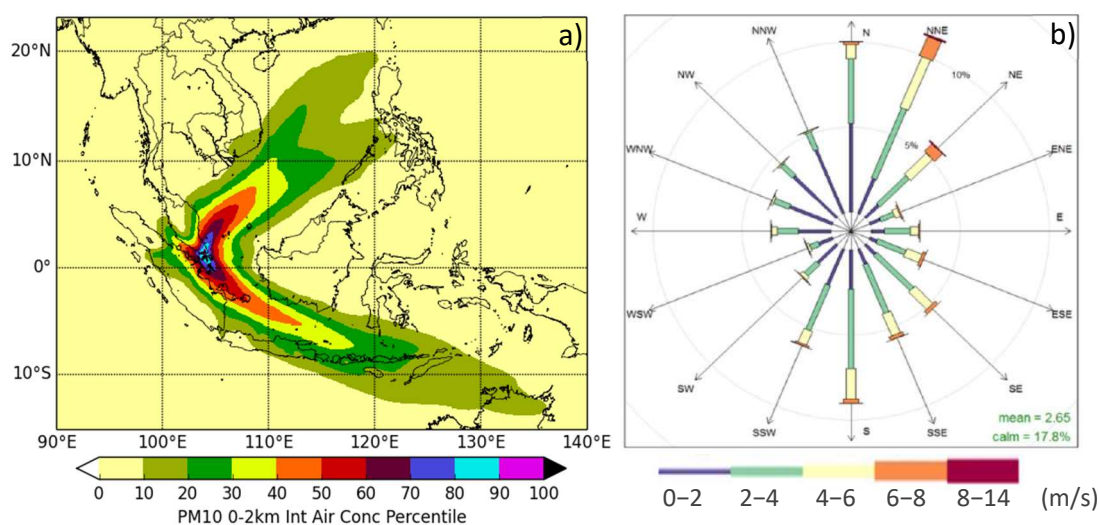


Figure 1. a) Air history backrun percentiles for 2010–2015. The coloured contours represent percentile levels for backrun air concentrations, b) Percentage of observed counts per wind direction and speed (1982–2016), Changi Climate Station.

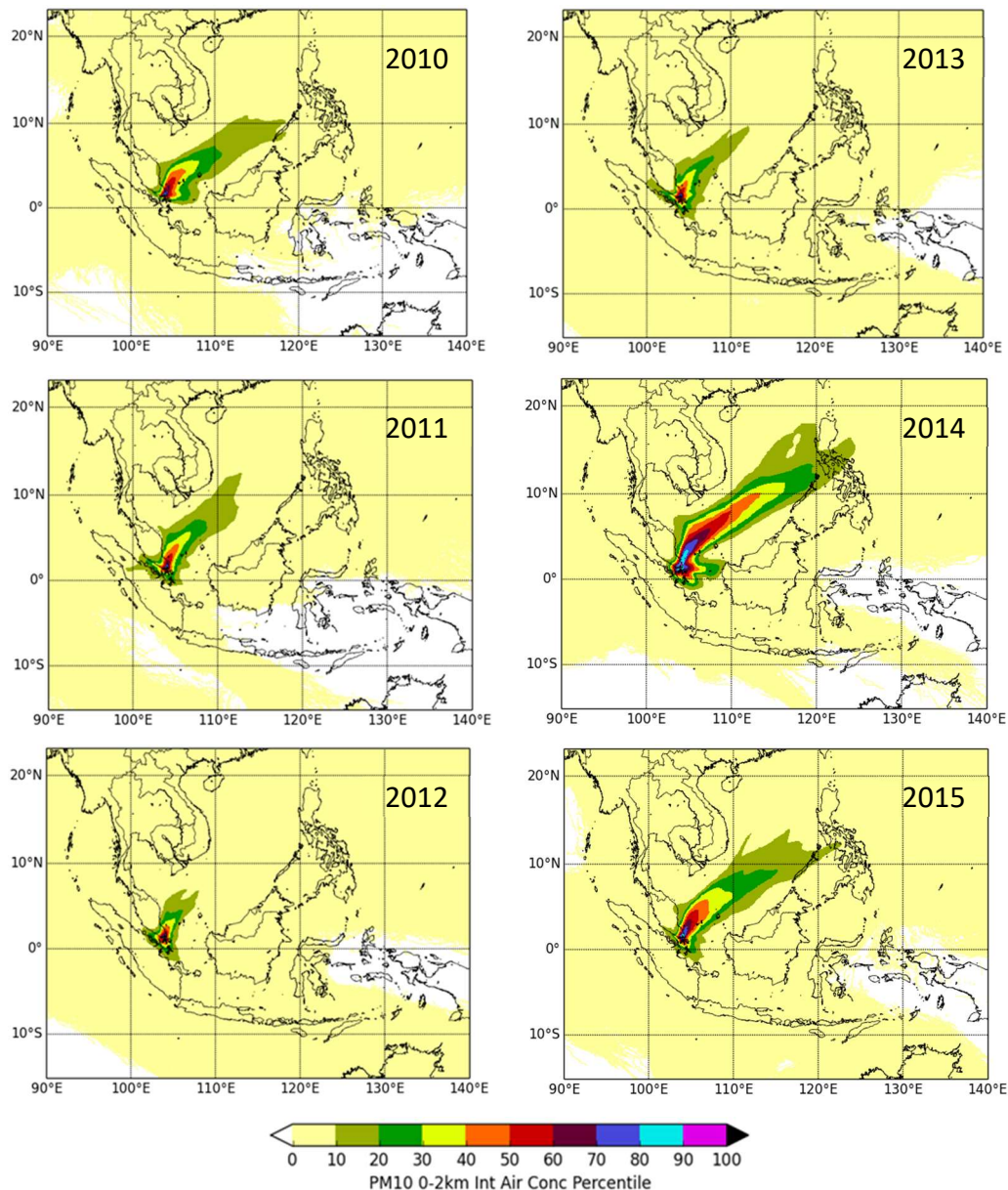


Figure 2. Percentile charts for FMA airflow history between 2010–2015, as in Fig. 1a.

with less than 1 mm of rainfall recorded at the Changi Climate Station (McBride et al. 2015). It is evident in the backrun maps below that FMA 2014 had anomalously strong northeasterly airflow components (middle lower row, Fig. 2), with 10th percentile values stretching deep into the South China Sea and the Philippines. Strong northeasterlies could have inhibited convective activity, exacerbated dry conditions, and resulted in an anomalously high airflow contribution from Pengerang, southern Johor, affecting Singapore that year. A brief poor air quality episode occurred in Singapore during early March 2014 (The Straits Times, 2014).

MAY-JUNE-JULY (MJJ)

During MJJ months, winds start to transition to the Southwest Monsoon regime in the region, with

winds over Singapore blowing primarily from the southeast/southwest directions. During this period, thunderstorms and wetter conditions develop over much of Continental Southeast Asia while drier conditions start to develop over Indonesia as the main rainband that constitutes the Inter-Tropical Convergence Zone (ITCZ) migrates north of the equator. From Fig. 3, the geographical areas of concern to Singapore's air quality during this period are mainly maritime areas in the Java Sea to the southeast of Singapore and coastal regions of Sumatra, such as Riau, Jambi, and South Sumatra. Other regions of Indonesia such as Kalimantan, contribute less to local air quality (below 10th percentile) during these months.

In 2013 MJJ, Singapore experienced a severe haze episode for two weeks in June (BBC, 2013). The air

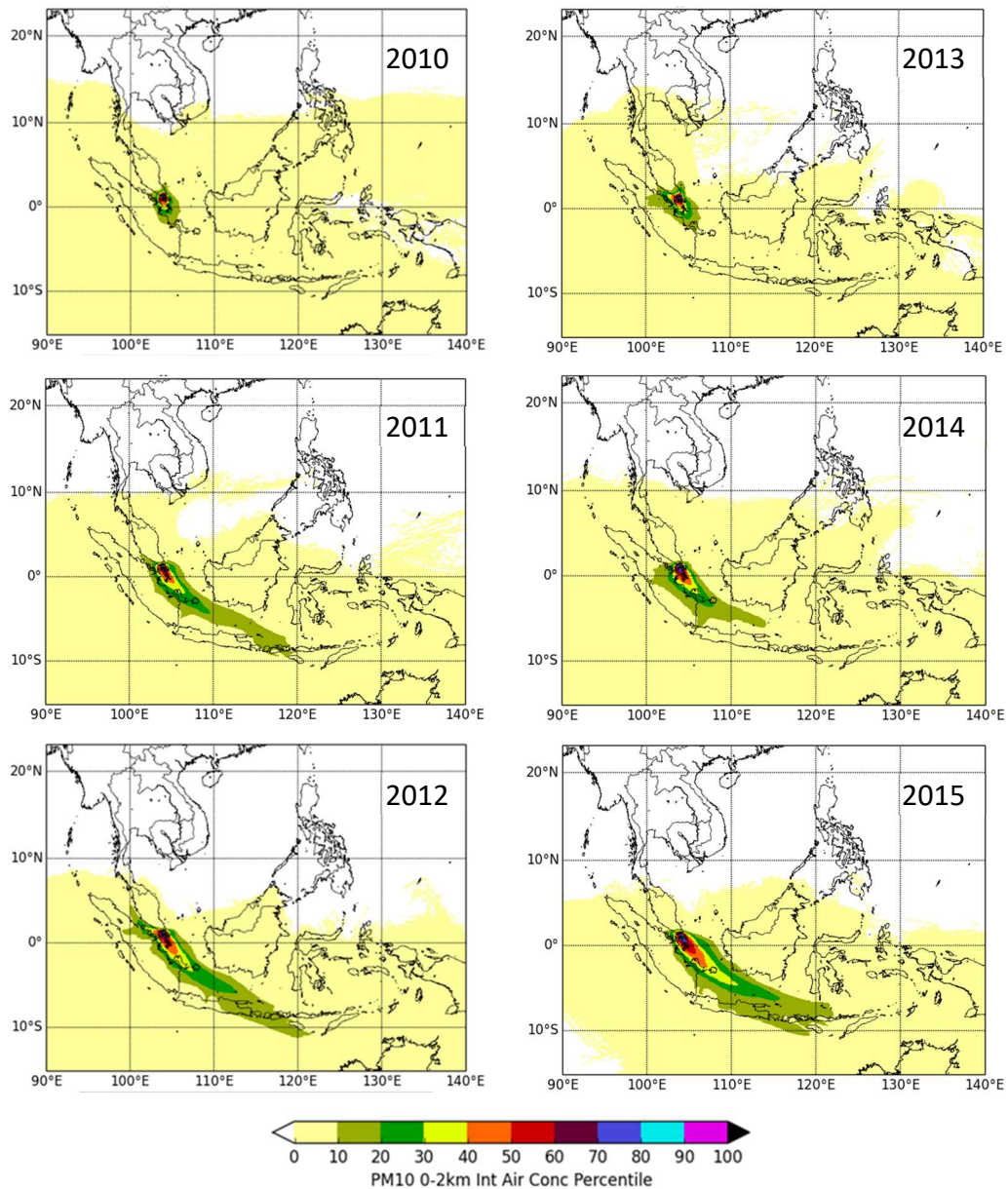


Figure 3. Percentile charts for MJJ airflow history between 2010–2015, as in Fig. 1a.

history analysis for MJJ 2013 in Fig. 3 shows anomalously higher source regions directly to the west of Singapore (10–30th percentile), such as the Malacca Strait and Riau province in Sumatra, and a lower contribution from the Java Sea region (below 10th percentile). The smaller source regions in 2013 (10th percentile or more), may be indicative of lighter winds and may have contributed to the extended length of the haze episode.

AUGUST-SEPTEMBER-OCTOBER (ASO)

The ASO period is when Southwest Monsoon conditions are at their strongest and is the traditional period where Singapore experiences its worst and longest stretches of haze. During these months,

extended dry periods can develop over Indonesia as the ITCZ migrates over Continental Southeast Asia. Figure 4 shows that in addition to regions in Sumatra, provinces further afield in South Kalimantan and East Java can also be potential geographical areas of concern for Singapore’s Air Quality (10–40th percentile) during this period.

During the years 2010, 2011, and 2012, dry conditions facilitated the development of poor air quality episodes over Singapore with contributions from eastern coastal provinces of Sumatra like Riau and Jambi. Backrun maps below also indicate that wind flow originated from these provinces (10–30th percentile) as well as maritime areas in the Java Sea during this period.

In 2014 and 2015, Singapore experienced poor air quality episodes with contribution from pollutant

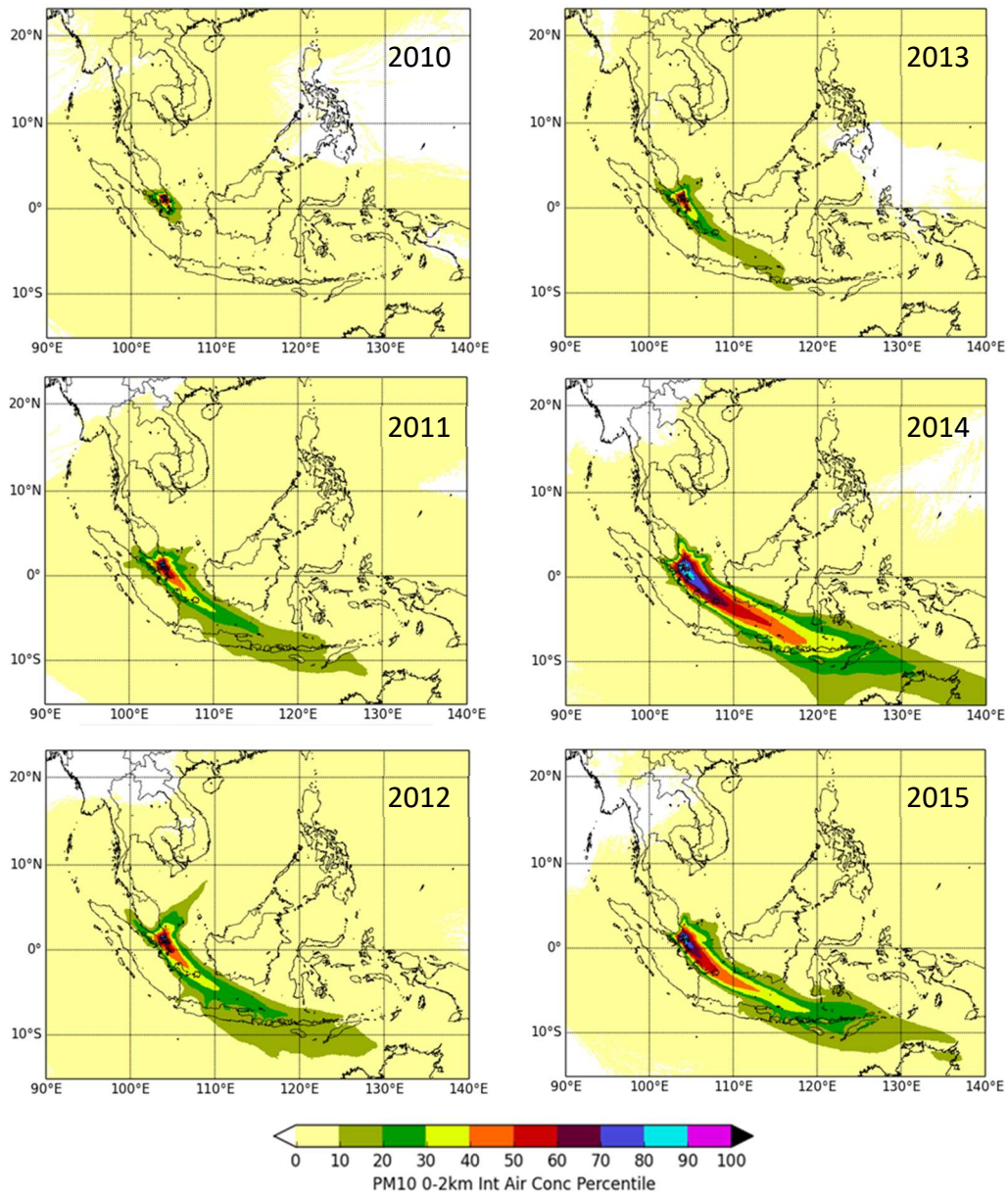


Figure 4. Percentile charts for ASO airflow history between 2010–2015, as in Fig. 1a.

sources in South Kalimantan. Backrun maps below show a higher contribution to airflow over Singapore from South Kalimantan in 2014 and 2015 (10–40th percentile) compared to other years (less than 10th percentile). El Niño conditions, which developed in the second half of 2014 and persisted in 2015, also exacerbated the dry conditions over Indonesia, southern Peninsular Malaysia, and Singapore and facilitated pollution emission events and transport. In particular, a period of severe haze affected much of Southeast Asia in 2015, resulting in a state of emergency being declared over Indonesia and schools being shut in Singapore, Malaysia, and Indonesia (The Straits Times, 2015).

Winds start to transition to the Northeast Monsoon regime during the November, December, and January period. Wet conditions develop over Peninsular Malaysia, Singapore, and Indonesia during this time as the main rainband associated with the ITCZ migrates southwards over the equator. The ensuing wetter conditions help to alleviate pollutant emission events and transport over these regions. Hence, no haze episode has affected Singapore during these months between 2010 and 2015. Dry conditions start to develop over continental Southeast Asia in countries such as Thailand, Myanmar, and Cambodia, but as Fig. 5 shows, air-flow over Singapore originating from these regions is not significant in NDJ (less than 10th percentile).

NOVEMBER-DECEMBER-JANUARY (NDJ)

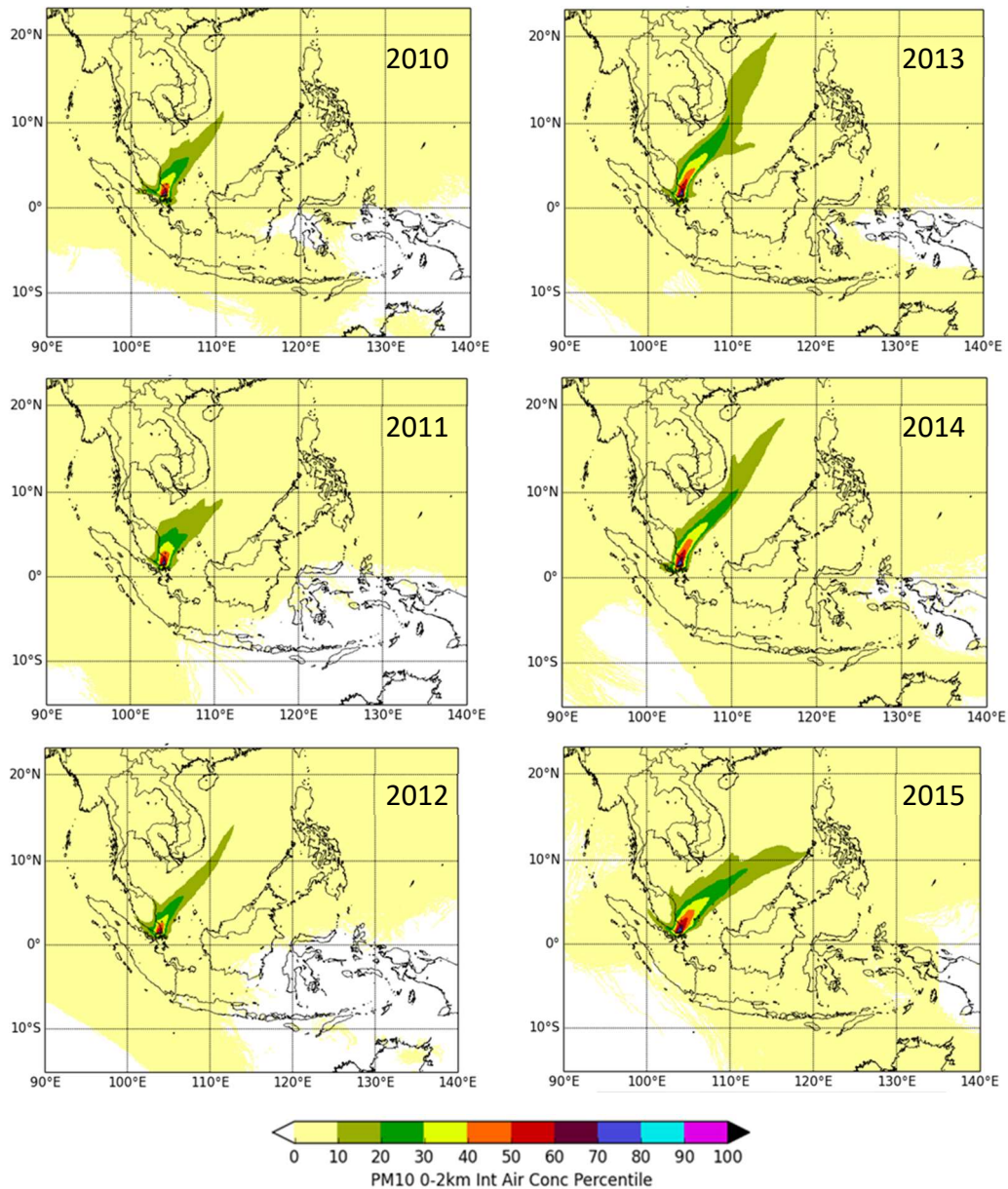


Figure 5. Percentile charts for NDJ airflow history between 2010–2015, as in Fig. 1a.

CONCLUSION

This air quality history study has provided a geographical perspective on the potential sources of pollutants from regional land and maritime areas around Singapore. Backruns using the NAME model were run daily for the period 2010–2015, driven by meteorological fields from the Global UM model. Substantial annual variation in air history maps exists between 2010 and 2015, which help explain varying air quality episodes that originate from different source regions year-to-year. Seasonal analysis of the air history maps also indicates that certain geographical regions pose a greater concern to Singapore’s air quality when

considered in tandem with weather conditions/anthropogenic activities during different times of the year. In terms of air quality monitoring in an operational context, the maps provide a guide for increased scrutiny on dry conditions developing in particular geographical regions, which may be potential pollutant sources during some months of the year.

While this study was conducted at near surface levels (0–2 km), primarily to assess the potential for transport of pollutants to Singapore in the atmospheric boundary layer, there is potential to extend this study further to include other levels of the atmosphere for other meteorological and hazard assessment purposes. For example, it is worth conducting a set of backruns for

an air history analysis at the atmospheric steering levels of 700–850 hPa, which is around 1.5–3 km above the earth's surface. Unlike pollutants which primarily reside in the planetary boundary layer, weather systems are advected and propagated at slightly higher levels of the atmosphere known as the steering level. Localised convective thunderstorms and larger organised storm systems like Sumatra squalls and monsoon surges often originate in areas beyond Singapore and propagate under the influence of steering level winds. By having a statistical study of steering level winds, a better understanding of seasonal source regions for storms that develop and propagate to Singapore will be obtained.

Forward runs of dispersion models like NAME are useful during a hazard release event where the locations of emission sources are known and the impact and spread of particles are to be assessed. On the other hand, conducting backruns with percentile computations post-event will complement the hazard analysis as they can help identify anomalous wind flows during the event which differ from long-term wind flow averages. Post-event backruns will help to isolate causes of severe weather episodes such as heavy rainfall events and dry spells or identify possible source regions for hazard release incidents.

Additionally, backruns of NAME could be conducted with different NWP models such as ECMWF, WRF and local models for sensitivity tests, and to provide validation and comparison for wind profiles derived across different models.

ACKNOWLEDGMENTS

UK Met Office for their guidance in NAME dispersion modelling studies.

REFERENCES

BBC (2013) Singapore haze hits record high from Indonesia fires. Available at: <http://www.bbc.com/news/world-asia-22998592>, last accessed: 1 March, 2018.

Davies, T. Cullen, M.J.P., Malcolm, A.J., Mawson, M.H., Staniforth, A., White, A.A., and Wood, N. (2005) A new dynamical core for the Met Office's global and regional modelling of the atmosphere. *Quarterly Journal of the Royal Meteorological Society*, 131:1759–1782.

Jones, A. (2004) Atmospheric dispersion modelling at the Met Office. *Weather*, 59: 311–316.

Madden, R.A. and Julian, P.R. (1971) Detection of a 40–50 Day Oscillation in the Zonal Wind in the Tropical Pacific. *Journal of the Atmospheric Sciences*, 28:702–708.

McBride, J.L., Sahany, S., Hassim, M.E.E., Nguyen, C.M., Lim, S.Y., Rahmat, R., Cheong, W.K. (2015) The 2014 Record Dry Spell at Singapore: An Intertropical Convergence Zone (ITCZ) Drought. *Bulletin of the American Meteorological Society*, 96:S126–S130.

NEA (2011) Executive Summary Report of the Advisory Committee on Ambient Air Quality, Advisory Committee on Singapore Ambient Air Quality. Available at: <http://www.nea.gov.sg/docs/default-source/anti-pollution-radiation-protection/air-pollution/executive-summary.pdf>, last accessed 1 March 2018.

Saji, N.H., Goswami, B.N., Vinayachandran, P.N., and Yamagata, T. (1999) A dipole mode in the Indian Ocean. *Nature*, 401:360–363.

The Straits Times (2014) PSI hits moderate range as haze hangs over Singapore on Sunday evening. Available at: <http://www.straitstimes.com/singapore/psi-hits-moderate-range-as-haze-hangs-over-singapore-on-sunday-evening-0>, last accessed: 01 Mar 2018.

The Straits Times (2015) Haze crisis set to be one of the 'worst on record'. Available at: <http://www.straitstimes.com/asia/haze-crisis-set-to-be-one-of-the-worst-on-record>, last accessed: 01 March 2018.

von Engeln A. and Teixeira, J. (2013) A Planetary Boundary Layer Height Climatology Derived from ECMWF Reanalysis Data. *Journal of Climate*, 17:6575–6590.

GLOSSARY

Boundary Layer (BL): The layer in the atmosphere close to the ground that is affected the most by the daily temperature cycle and where strong mixing occurs.

Constant Altitude Plan Position Indicator (CAPPI): A gridded product that shows a horizontal cross-section of data at a constant altitude or height.

Coordinated Universal Time (UTC): The primary standard time, similar to Greenwich Mean Time. Local time in Singapore is 8 hours ahead of the Coordinated Universal Time.

Data Assimilation (DA): Procedure through which observational data is used to update a NWP model.

Dipole Model Index (DMI): Index used to calculate the phase of the Indian Ocean Dipole based on the east-west sea surface temperature gradient over the Indian Ocean.

Dispersion model: A model based on mathematical equations of how air pollutants disperse in the atmosphere.

El Niño – Southern Oscillation (ENSO): Irregular variations in the winds and sea surface temperatures over the tropical Pacific Ocean (variations in the Walker Circulation). The pattern oscillates between neutral, El Niño, and La Niña with an average period of 3 to 5 years.

Ensemble Prediction System (EPS): A system where multiple forecasts are produced so that the uncertainty and most likely outcome of a weather forecast can be assessed.

Indian Ocean Dipole (IOD): The difference in sea surface temperature between the western Indian Ocean (Arabian Sea) and the eastern Indian Ocean (south of Indonesia), which oscillates irregularly

IndoSST: Sea surface temperature in the Indonesian seas (0° to 10°S, 90°E to 120°E).

Inter-monsoon (IM): The transitional periods between the Northeast and Southwest monsoons.

Intertropical Convergence Zone (ITCZ): A belt of low pressure near the equator where the trade winds from the Northern and Southern hemispheres meet, generally marked by extensive regions of convection.

Local time (LT): The time in Singapore.

Madden-Julian Oscillation (MJO): One of the most important fluctuations in tropical weather on weekly to monthly timescales. It is often characterised as a pulse of cloud and rain that moves eastward along the equator, typically occurring every 30-60 days.

Meteorological Service Singapore (MSS): Singapore's national authority on the weather and climate. Various entities under MSS include:

- **Weather Service Department (WSD):** The department under MSS that provides weather forecasts, warnings, and applied research.
- **Centre of Climate Research Singapore (CCRS):** The research arm of MSS.
- **Meteorological Systems Department (MSD):** Works to maintain MSS's operational and technical requirements.
- **Applied Modelling Branch (AMB):** Models various weather influenced hazards, such as haze and volcanic eruptions.
- **Climate Modelling and Prediction (CMP) branch:** Focuses on understanding tropical weather and climate processes, as well as climate change.

- Subseasonal and Seasonal Prediction (SSP) branch: Provides subseasonal and seasonal forecasts for Singapore and the surrounding Southeast Asia region.
- Weather Modelling and Prediction (WMP) branch: Focuses on improving weather forecasts, in particular Singapore's own SINGV model.
- Climate and Climate Studies (CCS) branch: In charge of collating and quality control of MSS's weather data.

Ministry of the Environment and Water Resources (MEWR): Ministry in Singapore that is committed to providing Singaporeans with a quality living environment. There are two statutory boards associated with MEWR:

- National Environment Agency (NEA): Organisation responsible for improving and sustaining a clean and green environment in Singapore, including meteorological services under MSS.
- Public Utilities Board (PUB): Singapore's national water agency.

Nino3.4: Index used to measure ENSO, based on sea surface temperatures in the tropical eastern Pacific.

Northeast (NE): Generally referring to the wind direction, or monsoonal flow during the boreal winter.

Numerical Atmospheric dispersion Modelling Environment (NAME) model: A dispersion model developed by the UK Met Office for a range of hazards and pollution monitoring purposes.

Numerical Weather Prediction (NWP): Computer models that solve mathematical equations representing atmospheric physics. Used extensively in weather forecasting.

Oceanic Niño Index (ONI): A 3-month running mean of the Nino3.4 index.

Prognostic Cloud and Condensate Scheme (PC2): A scheme or plan that predicts the cloud and condensate for a NWP model.

ScsSST: Sea surface temperature in the South China Sea (0° to 10°N, 100°E to 116°E).

Sea surface temperatures (SST): Water temperature close to the ocean's surface.

Singapore Variable Resolution (SINGV): MSS's integrated numerical weather prediction system, developed jointly in collaboration with the UK Met Office.

Southwest (SW): Generally referring to the wind direction, or monsoonal flow during the boreal summer.

SgP03: Average monthly rainfall for three Singapore stations that have records going back to 1956.

Sumatra squalls: A line of thunderstorms (squall) that originates near or over Sumatra, approaching Singapore from northwest to southwest direction.

PM10: Particle matter with a diameter less than 10 microns.

UK Met Office (UKMO): The United Kingdom's national weather service.

Unified Model (UM): A numerical model of the atmosphere developed by UK Met Office that is used for both weather and climate applications.

World Health Organisation (WHO): An agency under the United Nations with the primary role to direct international health and lead partners in global health responses.

World Meteorological Organisation (WMO): An agency under the United Nations for meteorology, both weather and climate, as well as operational hydrological services.



Website: ccrs.weather.gov.sg

Address: 36 Kim Chuan Road, Singapore